

Driftsstudie av Lav NO_x brennerteknologi

Kjartan Juul Skarbø

Master i energi og miljø

Innlevert: juni 2013

Hovedveileder: Terese Løvås, EPT

Norges teknisk-naturvitenskapelige universitet
Institutt for energi- og prosessteknikk

EPT-M-2013-62

MASTER THESIS

for

Stud.techn. Kjartan Juul Skarbø

Spring 2013

Operation study of Low NOx burner technology*Driftsstudie av Lav NOx brennerteknologi***Background and objective**

The challenges related to climate changes are in large believed to be caused by increased CO₂ emissions from combustion processes in the industry, power and transportation sectors. The use of hydrogen or hydrogen enriched-fuels is one of the methods to reduce greenhouse gas emission from combustion. Employing pure hydrogen is considered a promising approach within carbon capture and storage (CCS) technologies, as the carbon is sequestered from the hydrocarbon fuel resulting in zero CO₂ emissions from the combustion process. This technology is foreseen used in both boiler systems and turbines for power production. Yet the use of hydrogen as a fuel represents significant challenges related to the design of the burner and the combustion chamber due to high combustion temperatures. In addition, hydrogen combustion is usually associated with higher levels of unwanted NO_x emissions due to the increased temperatures in the burning zone. NO_x emissions are responsible for smog and poor air quality and should be avoided.

The project aims to study non-linear effects of combustion conditions on NO_x emissions in a low-NO_x burner and to establish optimum operating setting for low NO_x conditions.

The work is related to the activities within the international research centre BIGCCS, and is in close collaboration with Sintef Energy AS. The work is a continuation of the candidate's project thesis.

The following tasks are to be considered:

1. Literature study based on results from project thesis.
2. Planning measurement campaign based on central composite design.
3. Measurements of emission levels varying up to 5 different operating parameters.
4. Analysis of data and identification of optimal operating settings for low NO_x conditions.

Within 14 days of receiving the written text on the master thesis, the candidate shall submit a research plan for his project to the department.

When the thesis is evaluated, emphasis is put on processing of the results, and that they are presented in tabular and/or graphic form in a clear manner, and that they are analyzed carefully.

The thesis should be formulated as a research report with summary both in English and Norwegian, conclusion, literature references, table of contents etc. During the preparation of the text, the candidate should make an effort to produce a well-structured and easily readable report. In order to ease the evaluation of the thesis, it is important that the cross-references are correct. In the making of the report, strong emphasis should be placed on both a thorough discussion of the results and an orderly presentation.

The candidate is requested to initiate and keep close contact with his/her academic supervisor(s) throughout the working period. The candidate must follow the rules and regulations of NTNU as well as passive directions given by the Department of Energy and Process Engineering.

Risk assessment of the candidate's work shall be carried out according to the department's procedures. The risk assessment must be documented and included as part of the final report. Events related to the candidate's work adversely affecting the health, safety or security, must be documented and included as part of the final report. If the documentation on risk assessment represents a large number of pages, the full version is to be submitted electronically to the supervisor and an excerpt is included in the report.

Pursuant to "Regulations concerning the supplementary provisions to the technology study program/Master of Science" at NTNU §20, the Department reserves the permission to utilize all the results and data for teaching and research purposes as well as in future publications.

The final report is to be submitted digitally in DAIM. An executive summary of the thesis including title, student's name, supervisor's name, year, department name, and NTNU's logo and name, shall be submitted to the department as a separate pdf file. Based on an agreement with the supervisor, the final report and other material and documents may be given to the supervisor in digital format.

- Work to be done in lab (Water power lab, Fluids engineering lab, Thermal engineering lab)
 Field work

Department of Energy and Process Engineering, 16. January 2013



Olav Bolland
Department Head



Terese Løvås
Academic Supervisor

Research Advisors: Mr. Marcin Dutka (EPT) and Dr. Mario Ditaranto (Sintef Energy).

Preface

This the Master's Thesis of Kjartan Juul Skarbø on Low NO_x burner technology. The work was carried out the spring of 2013, related to the activities within the international research centre BIGCCS and in close collaboration with SINTEF Energy AS.

Trondheim 2013-06-10

A handwritten signature in black ink, reading "Kjartan Juul Skarbø". The signature is written in a cursive, flowing style.

Kjartan Juul Skarbø

Acknowledgements

I want to thank my research advisor Marcin D. Dutka (EPT) for his cooperation and guidance from the very start in September 2012. The project could never be realised without technical help at the laboratory, particularly from Halvor Flatberg and Stein Kristian Skånøy. I would also like to thank my academic supervisor Terese Løvås (EPT) and research advisor Mario Ditaranto (SINTEF).

Summary

The formation of NO_x in combustion is a complex process. It can be categorised into three mechanisms; thermal NO_x, prompt NO_x and NO_x from fuel containing nitrogen. The importance of the mechanisms in this report is respectively. When fuels are enriched by hydrogen, the flame temperature may rise and increase the thermal NO_x formation.

In this thesis, combustion of methane and hydrogen mixtures is investigated in the partial premixed bluff-body burner (a low-NO_x burner) from SINTEF. Five independent operation variables are investigated by applying the response surface methodology. These are power, equivalence ratio of air, fuel composition, secondary fuel injection and the position of the burner head. The multiple combinations of these parameters give a wide range of NO_x emission and flame stabilities.

It was found that the overall NO_x emissions from the burner proved to be low and that the emissions could be significantly reduced further by lowering the burner head (L2). Compared to other low-NO_x burners, the results are promising, but need further experiments to verify the findings in this report.

Sammendrag

NO_x dannelsen i forbrenning er en komplisert prosess. Den kan bli kategorisert i tre mekanismer; termisk NO_x, hurtig NO_x og NO_x fra nitrogenforbindelser i drivstoffet. Betydning av mekanismene i denne rapporten er henholdsvis. Forbrenning av hydrogen gir høyere flammtemperaturer som igjen kan føre til mer produksjon av termisk NO_x.

En lav-NO_x brenner utviklet av SINTEF er testet for forskjellige blandinger av metan og hydrogen gass. Fem uavhengige operasjonsfaktorer er undersøkt ved å benytte en velkjent optimeringsmetode kalt «response surface methodology». De fem parameterne er termisk effekt, mengde hydrogen blandet med metangass, mengde ekstra lufttilførsler, sekundær brennstoff injeksjon og posisjonen til brennerhodet. Hvordan de mange kombinasjonene av disse faktorene spilte inn på NO_x-dannelsen ble undersøkt.

Det ble konkludert med at brenneren ga lave utslipp av NO_x generelt og at de kunne bli redusert betydelig ved å senke høyden til brennerhodet (L2). Sammenlignet med andre lav-NO_x brennere virker resultatet i denne rapporten lovende, men flere eksperimenter trengs for å underbygge disse.

Table of Contents

Preface	I
Acknowledgements	IV
Summary	V
Sammendrag	VI
List of Figures	X
List of Tables	XI
Introduction	1
1. NO_x	2
1.1. Health and Environment.....	2
1.2. Formation of NO _x	3
1.2.1. Prompt NO _x Formation.....	3
1.2.2. Formation from fuel	3
1.2.3. Zeldovich mechanism – thermal NO _x	4
1.3. NO _x -reducing technologies.....	5
1.3.1. Pre-combustion.....	5
1.3.2. Post-combustion	5
1.4. Low-NO _x burners.....	6
1.4.1. Overview	6
1.4.2. The PPBB-burner	7
2. Design of experiment	11
2.1. Response surface methodology	11
2.1.1. Full factorial design.....	11
2.1.2. Central Composite Design (CCD)	12
2.1.3. Choice of α	13
2.2. Regression analysis.....	14
2.2.1. The regression function.....	14

2.2.2.	Assumptions for linear regression.....	15
2.2.3.	Residual plots	16
2.2.4.	R ² -values and lack-of-fit test.....	17
2.2.5.	Modelling	17
3.	Theory of errors.....	18
3.1.	Introduction	18
3.2.	Types of errors.....	18
3.2.1.	Systematic error.....	18
3.2.2.	Uncertainties and random error.....	18
3.3.	Propagation of errors	19
4.	Method of measurement	20
4.1.	Equipment.....	20
4.1.1.	Mass Flow controllers	20
4.1.2.	Gas analysers.....	20
4.1.3.	Temperature Probes.....	21
4.2.	Setup	22
4.3.	Procedure	23
5.	Investigation of errors.....	24
5.1.	Human errors	24
5.1.1.	Configuration of sampling gas	24
5.2.	Systematic deviations	25
5.2.1.	Leakage diluting gas samples.....	25
5.2.2.	Real flow from MFCs	25
5.2.3.	Calibration of MFC	27
5.2.4.	Factors of short ranges	27
5.2.5.	Summary	28
6.	Results.....	29
6.1.	The hydrogen lance	29
6.1.1.	2 nd Matrix	29

6.1.2.	1 st Matrix	36
6.2.	The methane lance	40
6.2.1.	1 st Matrix	41
7.	Discussion	45
7.1.	The 2 nd matrix of the hydrogen lance	45
7.1.1.	R2 - Fuel to secondary holes	45
7.1.2.	L2 - Height of burner head	46
7.1.3.	H2 – Mass fraction of hydrogen.....	47
7.1.4.	λ or Lambda – Amount of excess air	48
7.1.5.	Power.....	48
7.2.	The Two Lances	48
7.3.	Overall performance	49
8.	Conclusion	50
9.	References.....	51
10.	Appendix.....	52

1. List of Figures

Figure 1.1 – Contributions to NO _x Emissions in 2010 (European Environment Agency (EEA)).....	3
Figure 1.2 - k ₁ as a function of temperature	5
Figure 1.3 – PPBB burner (SINTEF)	7
Figure 1.4 – Two heights of L ₂	8
Figure 1.5 – 9 mm L ₂	8
Figure 1.6 – 20 mm L ₂	8
Figure 1.7 - Air Velocity	9
Figure 2.1 – 2 levels 2 factors design.....	11
Figure 2.2 – 3 levels 2 factors design.....	11
Figure 2.3 - CCD for three factors	12
Figure 2.4 – Spherical Design	13
Figure 2.5 - Residual Plots Example.....	16
Figure 4.1 – Gasmet DX4000	20
Figure 4.2 - HORIBA PG-250A	21
Figure 4.3: Burner head from ignition opening	21
<i>Figure 4.4 – Configuration of the test rig</i>	<i>22</i>
Figure 4.5 – Overview of the rig	23
Figure 4.6 - Control Panel (LabView)	23
Figure 6.1 – NO _x response for 2 nd Matrix	29
Figure 6.2 – Coded significance of terms	31
Figure 6.3 - Residual Plots, 2 nd Matrix, Hydrogen Lance	32
Figure 6.4 – High Hold values, 2 nd Matrix Hydrogen Lance.....	33
Figure 6.5 - Low Hold Values, 2 nd Matrix Hydrogen Lance	34
Figure 6.6 – CO levels, 2 nd Matrix Hydrogen Lance	35
Figure 6.7 – No _x and CO, 1 st Matrix Hydrogen lance.....	37
Figure 6.8 - Significance of terms, 1 st Matrix, Hydrogen lance.....	37
Figure 6.9 - Residual Plots, 1 st Matrix, Hydrogen Lance.....	39
Figure 6.10 – Contour Plots for 1 st Matrix, Hydrogen lance	40
Figure 6.11 – No _x and CO, 1 st Matrix Methane lance.....	41
Figure 6.12 – Significance of terms, 1 st Matrix, Methane lance.....	42
Figure 6.13 - Residual Plots, 1 st Matrix, Methan Lance	43
Figure 6.14 – Contour Plots for 1 st Matrix, Methane lance	44

2. List of Tables

Table 1.1 - Commercial Available Low NOx fan burners for natural gas	6
Table 1.2 – The five factors	10
Table 2.1 – Full factorial runs	12
Table 2.2 – CCD runs.....	13
Table 2.3 – Full quadratic model example.....	15
Table 4.1 – Mass Flow Controllers	20
Table 5.1 – Fuel difference	26
Table 5.2 – Calibration of MFCs	27
Table 6.1 – Table of factors, 2nd Matrix	29
Table 6.2 - Full quadratic model of 2 nd Matrix Hydrogen Lance	30
Table 6.3 – Final model for 2 nd Matrix, Hydrogen Lance	31
Table 6.4 - Regression analysis for CO	35
Table 6.5 – Table of factors, 1st Matrix.....	36
Table 6.6 - Full quadratic model of 1 st Matrix Hydrogen Lance	38
Table 6.7 – Final model for 1 st Matrix, Hydrogen lance.....	39
Table 6.8 – Full quadratic model for 1 st Matrix, Methane lance	42
Table 6.9 – Final model for 1 st Matrix, Methane Lance	43
Table 6.10 - Velocity of air	46

Introduction

Carbon-capture storage technologies have different approaches. By extracting hydrogen from hydrocarbons and burning it, CO₂ is avoided in the exhaust. However, combustion of hydrogen has challenges related to burner and combustion chamber design, as well as NO_x emissions, due to high combustion temperatures. NO_x emissions are an unwanted side effect of combustion causing risk to health and environment.

This thesis is an operation study of a low-NO_x burner from SINTEF. The response surface methodology is applied to investigate how up to five independent operating variables affect the NO_x emission of the burner.

1. NO_x

1.1. Health and Environment

NO_x is a collective term for nitrogen oxides. NO and NO₂ are by far the most common forms. If NO is released in the ambient, it quickly oxidises to NO₂. When the emissions of NO_x are given in mass, it is often referred to the molecular mass of NO₂.

There are several health and environment effects related to NO_x. It proven to cause for example acid rain, smog and production of near ground poisonous ozone (Muzio and Quartucy, 1997). There are many negative health effects from NO_x (EPA):

NO_x react with ammonia, moisture, and other compounds to form small particles. These small particles penetrate deeply into sensitive parts of the lungs and can cause or worsen respiratory disease, such as emphysema and bronchitis, and can aggravate existing heart disease, leading to increased hospital admissions and premature death.

The compounds are classified as air pollutants and the emission of NO_x is regulated by law, like the Clean Air Act Amendments of 1990 in the US. NO and NO₂ has a short lifetime in the atmosphere and is considered as a local pollution. N₂O is another nitrogen oxide that has a much longer lifetime, and therefore a global problem contributing to climate change (Muzio and Quartucy, 1997).

1.2. Formation of NO_x

NO_x is formed naturally in the nature from lightening, but pollution from combustion is the main source (Muzio and Quartucy, 1997).

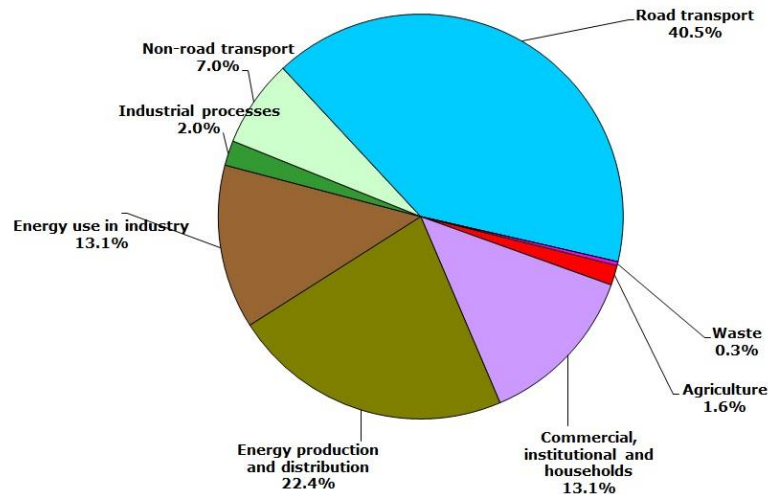


Figure 1.1 – Contributions to NO_x Emissions in 2010 (European Environment Agency (EEA))

Figure 1.1 illustrates how the transportation sector contributes the most to emission of NO_x, followed by emissions from commercial and industrial energy production. The formation of NO_x can be categorized into three mechanisms.

1.2.1. Prompt NO_x Formation

The prompt mechanism form nitrogen oxides when hydrocarbon radicals from the fuel react with nitrogen from the air. It was first identified by Fenimore in 1971. The radicals are found in the flame front and reacts with nitrogen promptly, hence the name. The mechanism is not as dependent on temperature, but rather the concentration of radicals. Prompt NO_x formation is therefore stronger for fuel rich conditions.

1.2.2. Formation from fuel

Chemical compounds in the fuel containing nitrogen can be oxidized to form NO_x. This only concerns certain liquid and solid fuels like coal. This type of formation of NO_x can be avoided by switching fuels, to for example natural gas.

1.2.3. Zeldovich mechanism – thermal NO_x

Air consists of about 78 percent nitrogen. If the temperature in the flame is high enough, the triple bond between the two nitrogen atoms in N₂ breaks. The free nitrogen radicals then react to intermediate compounds and eventually form NO_x. The thermal Zeldovich mechanism describes how NO is formed in higher temperatures. While prompt NO_x is formed instantly in early combustion stage by fuel radicals, the thermal mechanism is slower and occurs in latter stages.

The chemical kinetics of NO formation is complicated, but the mechanism is described as follows by (Warnatz et al., 2006):



The first reaction is the limiting step due to its high activation energy. The strong triple bonds in N₂ require high energy levels to break. When NO and a nitrogen radical is formed, it can be assumed that the radical immediately reacts like equation (2) and (3) illustrate. The rate of formation for NO can therefore be reduced to following equation.

$$\frac{d[NO]}{dt} = 2k_1[O][N_2] \quad (4)$$

The reaction rate constant, k_1 , is the one for equation (1).

$$k_1 = 1,8 \cdot 10^8 \exp\left(\frac{-318000}{RT}\right) \left[\frac{m^3}{mol \cdot s}\right] \quad (5)$$

Equation (4) shows that NO formation, thus NO_x, can be minimised by reducing the concentrations of oxygen-atom and nitrogen, the rate constant by lower temperature and the time of exposure (dt) or residence time.

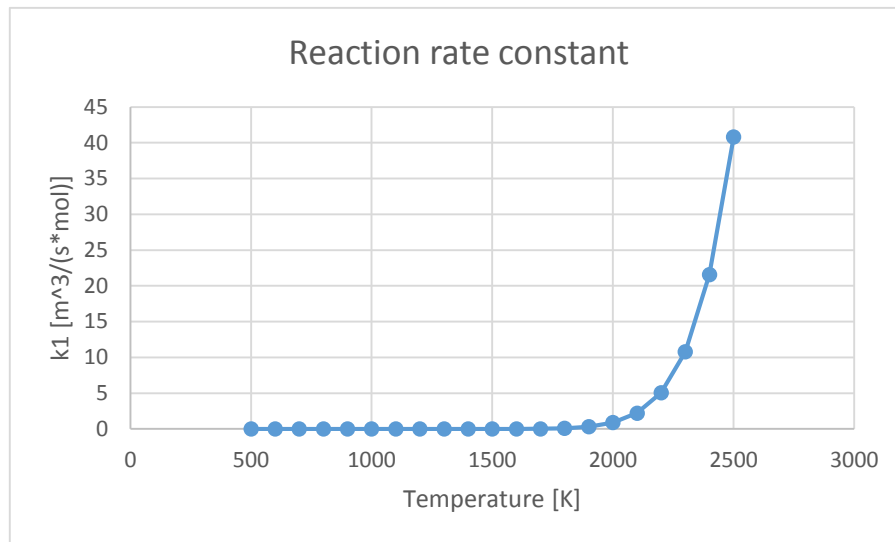


Figure 1.2 - k1 as a function of temperature

Figure 1.2 illustrate why the Zeldovich mechanism is referred to as the thermal NOx formation. It can be assumed that this mechanism does not contribute to any NOx formation for temperature below 1700 Kelvin.

1.3. NOx-reducing technologies

As mentioned, the most common source of NOx is combustion. A lot of research has been done to reduce the emissions (Skalska et al., 2010). Combustion occurs on a wide range of technics and scale. The amount of strategies to reduce NOx emissions is therefore extensive, but they all try to avoid the described mechanisms of formation.

1.3.1. Pre-combustion

Reduction in pre-combustion means to optimise the reactants of the combustion process to produce as little NOx as possible. NOx can be significantly reduced by changing fuel from nitrogen-rich coal to cleaner natural gas. As equation (4) shows, the rate of formation of NO is dependent on the concentration of nitrogen. Research has been done to eliminate the concentration further by burning fuels with pure oxygen, rather than air. This method is related to stationary facilities capable to extract the oxygen from the air. It is found that NOx emission per unit energy is less for oxy-fuels (Buhre et al., 2005).

1.3.2. Post-combustion

NOx can be extracted from the exhaust gas by for example selective catalytic process, thermal de-NOx or REPREENox (Miller and Bowman, 1989). Thermal de-NOx is here referred to a selective catalytic reduction process by ammonia. It is researched extensively and has the advantage that no waste is generated, like

absorption and adsorption processes do. It may reduce NO_x content by 85 % and is the most commonly used process (Skalska et al., 2010). Combining this technology with oxy-fuels can be beneficial due to the low volume rate of exhaust from the oxy-fuel combustion.

1.4. Low-NO_x burners

1.4.1. Overview

Table 1.1 shows some commercial available low-NO_x burners and their specifications. Low NO_x burners (LNB) are designed to minimise the thermal and prompt NO_x during combustion. In turbulent combustion, these mechanisms are very complex and hard to predict. LNBs adjust the combustion parameters by its geometry and operational control to create combustion zones that inhibits thermal NO_x. This can be achieved by mixing the oxidizer and fuel well so that no fuel-rich and high temperature region occurs in the flame. The burner design often becomes more complicated as the maximal power increases (Spangelo,

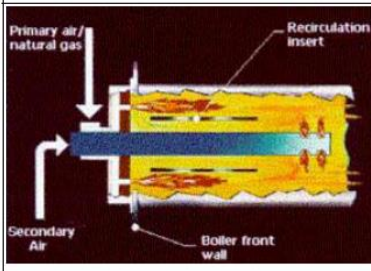
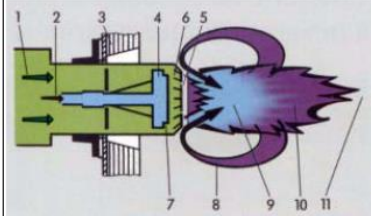
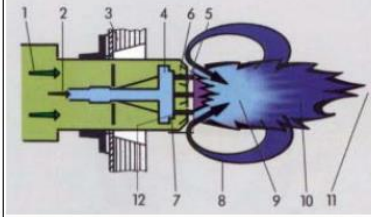
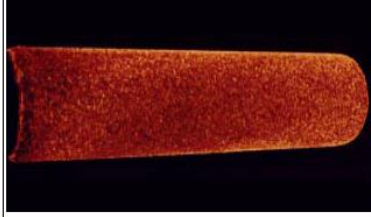

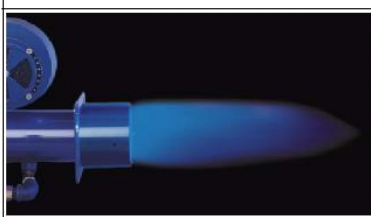
	Description
	<p>Johnston Boiler and GTI: FIR Burner</p> <ul style="list-style-type: none"> • Premixed • Staged Air • Internal FGR • Interstage heat removal • NO_x emission < 10 ppm • Turn down ratio: 1:4 • Capacity: 0.5 - 10 MW • Fuel pressure: 0.345 bar <p>http://www.johnstonboiler.com/</p>
	<p>Walter Dreizler GmbH: ARZ burner</p> <ul style="list-style-type: none"> • Internal FGR (8) • 2 combustion zones (7 and 9) • NO_x emission < 40 ppm (80 mg/kWh) • Turn down ratio: 1:10 • Capacity: 0.025 - 15 MW <p>http://www.dreizler.com/</p>
	<p>Walter Dreizler GmbH: ARZ Super burner</p> <ul style="list-style-type: none"> • Internal FGR (8) • 2 combustion zones (7 and 9) • Additional fuel staging (12) • NO_x emission < 30 ppm (60 mg/kWh) • Turn down ratio: 1:10 • Capacity: 0.025 - 15 MW <p>http://www.dreizler.com/</p>
	<p>Walter Dreizler GmbH: MAGMA burner</p> <ul style="list-style-type: none"> • Enhanced radiative heat transfer by use of ceramic burner (infrared-combustion) • Surface temperature of 700 to 900 °C. • NO_x emission 5 - 18 ppm (10 - 35 mg/kWh) • Capacity: 0.01 - 5 MW <p>http://www.dreizler.com/</p>
	<p>Power Flame: NOVA Plus burner</p> <ul style="list-style-type: none"> • Premixed • Enhanced radiative heat transfer by use of metallic porous mesh burner head • Flame stabilized on surface of porous mesh • NO_x emission < 9 ppm • Capacity: 0.6 - 4.3 MW • Fuel supply pressure: 0.045 - 0.070 bar <p>http://www.powerflame.com/</p>
	<p>Power Flame: NOVA premix burner</p> <ul style="list-style-type: none"> • Premixed • Swirl stabilized flame • NO_x emission < 30 ppm • Further reduction of NO_x (< 20 ppm) by increasing excess air • Capacity: 120 - 650 kW • Fuel supply pressure: 0.017 - 0.029 bar <p>http://www.powerflame.com/</p>

Table 1.1 - Commercial Available Low NO_x fan burners for natural gas

(Spalangelo, 2004)

2004). Some burners use flue gas recirculation (FGR) and staged combustion. These technics are able to reduce the maximal flame temperature and NO_x emission significantly, but at higher maintenance and installation costs. Burners that mix the fuel and oxidiser before the combustion chamber (premix) are exposed to the risk of flashback. This limits the application in the industry due to safety. Another concept is the swirl burner. It provides air with angular momentum to burn methane or hydrogen in a lean flame (Yegian and Cheng, 1998). It has proven to produce stable and robust flame with low emissions of NO_x and CO with the same efficiencies as present day industrial burners. The burner is installed in several hundred sites for different industries. The NO_x emission for this burner range from 5-40 ppm (at 3% O₂ in exhaust).

1.4.2. The PPBB-burner

The partial premix bluff-body burner from SINTEF mixes fuel and air along 17.3 mm; see Figure 1.3. The flame stabilise on the top of the burner head. The burner was manufactured in Switzerland to meet industrial standards.

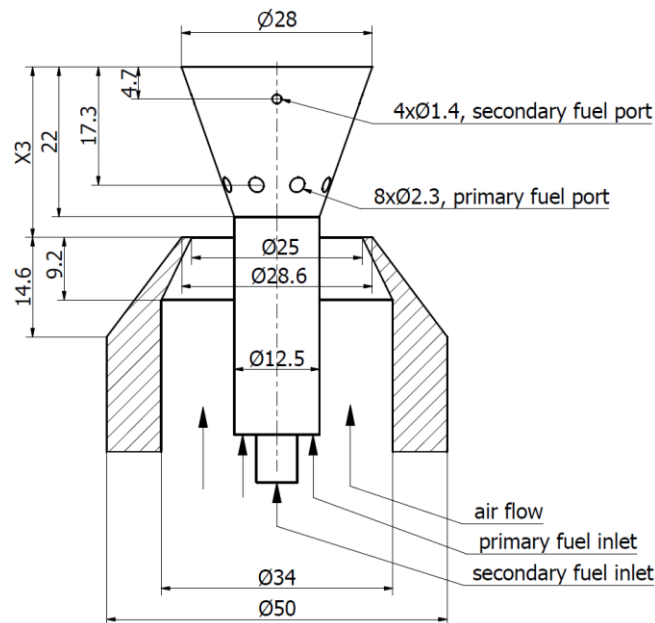


Figure 1.3 – PPBB burner (SINTEF)

The burner is designed for flame stabilisation behind the bluff body. Air flows through the converging section with increasing velocity and mixed with the fuel at the fuel ports. There are two types for ports for primary fuel and secondary fuel. Primary fuel is provided through eight equally distributed holes around the lower end of the bluff body. The secondary fuel is provided through four equally distributed holes around the upper part of the bluff body. Air and fuel is mixed in this section, and stabilises on top of the bluff body for combustion. The height

of the burner head (X3 in Figure 1.3) is adjustable during operation. This parameter will change the velocity of air and the whole mixing process of fuel and air. The height will be referred in this report as L2 [mm].

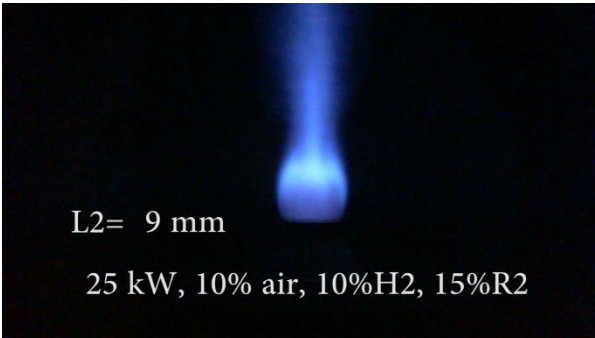
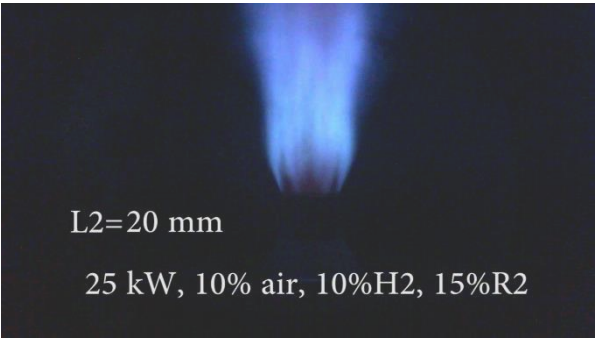


Figure 1.6 – 20 mm L2

Figure 1.5 – 9 mm L2

Figure 1.4 illustrates two different settings of the height of the burner head, L2. It is adjustable with a wrench beneath the burner while burning. The shape of the flame will change dramatically, as Figure 1.6 and Figure 1.5 illustrate.

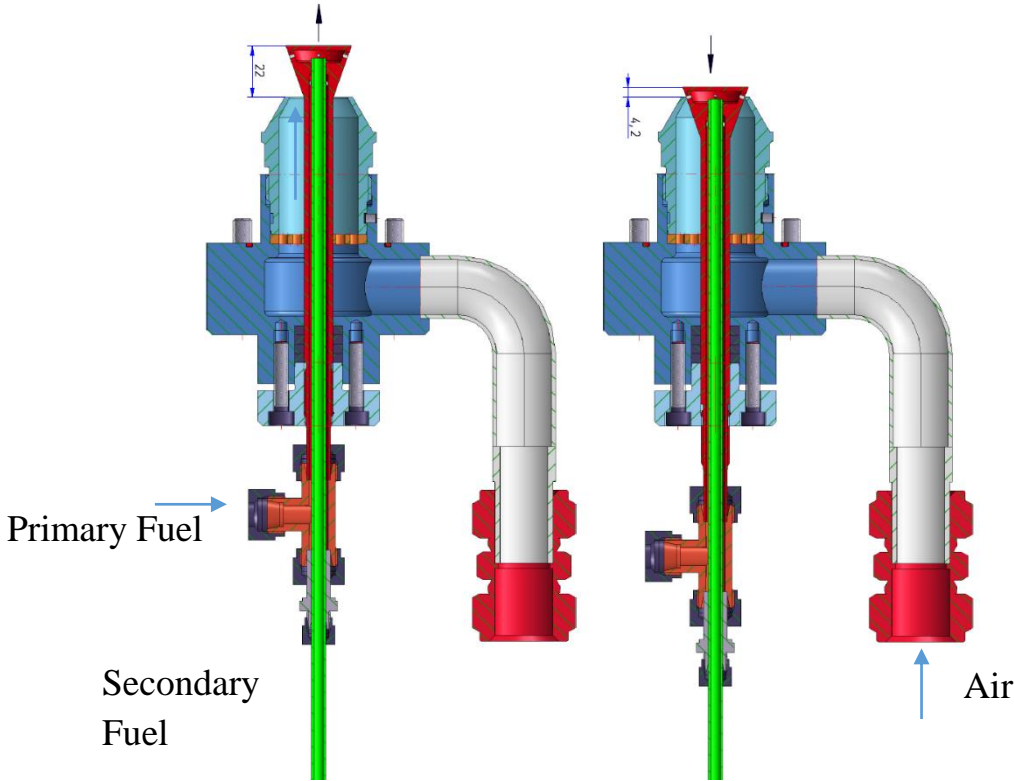


Figure 1.4 – Two heights of L2

From Figure 1.3 the relationship between the height of the burner L2 and the area of the outlet for air can be formulated as

$$A = \pi \left(12,5^2 - \left(14 - \frac{31}{88} L2 \right)^2 \right) [mm^2] \quad (6)$$

L2 is expressed in millimetres. The velocity of air can then be expressed as a function of air provided and the distance L2.

$$v = \frac{50 \cdot z}{3\pi \left(156,25 - \left(14 - \frac{31}{88} L2 \right)^2 \right)} [m/s] \quad (7)$$

Z is litres of air provided per minute and L2 is still expressed in millimetres. As for Figure 1.6 and Figure 1.5, the velocity of air was around 21 and 58 metres per second respectively at the outlet. A plot of velocities is illustrated in Figure 1.7 below.

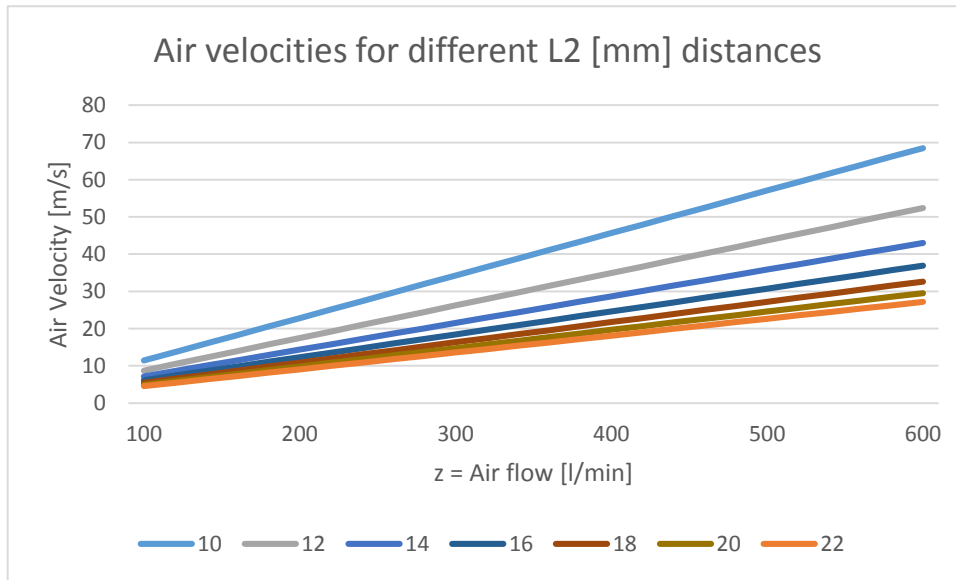


Figure 1.7 - Air Velocity

The fuel composition is the same for both secondary and primary fuel holes. The amount of fuel provided to the secondary holes (R2) is described as a percentage of the total flow of fuel in this report.

Air flows independently from the fuel settings. The amount of air is described with the air to fuel equivalence ratio (λ or lambda). In Figure 1.6 and Figure 1.5 the percentage are indicating how much air is provided over the stoichiometric requirement. Lambda is 1.10 in both cases.

Factor	L2	R2	λ/Lambda	H2	P
Unit	mm	%	-	wt%	kW

Table 1.2 – The five factors

Table 1.2 shows the adjustable factors for the burner. The fuel composition (H2) is the mass fraction of hydrogen in the methane-hydrogen mixture, but is referred to as the weight percentage. The burner can operate from 8 kW up to 25 kW.

This report will not go into the detailed chemical kinetics and turbulent combustion modelling. However, the burner allows to adjust R2, L2 and lambda to optimise the combustion process for different types of fuel and power. The concept is that the geometry of the burner head creates a recirculation zone behind the bluff body. The intent of the design is to avoid the temperature spikes during combustion thus reducing NO formation due to the Zeldovich mechanism. Response surface methodology is conducted to optimise the burner settings for lowest NO_x and CO emissions.

2. Design of experiment

2.1. Response surface methodology

Response surface methodology (RSM) is a term for a group of experiment design. The goal is to optimise an outcome by combining a number of factors that may have quadratic effect on the response. These effects has its origin in some unknown physical mechanisms (Myers et al., 2011). The method is widely used in the industry and is proven very efficient to obtain optimum combination of relevant factors. A screening experiment is often conducted first. It gives an overview of how the factors influence the result or response. When there is an idea of where the optimal point of operation might be, a more thorough second-order experiment within that region is designed. This way of quickly narrowing down the desired area, instead of investigating every point and combination, makes the method time- and cost-efficient in many cases.

2.1.1. Full factorial design

Full factorial design measures all combination of every level of every factor, defined in the design. If an experiment consists of two factors ($k=2$), and each factor has two levels ($N=2$), then $2^2 = 4$ runs are required, as Figure 2.1 illustrates.

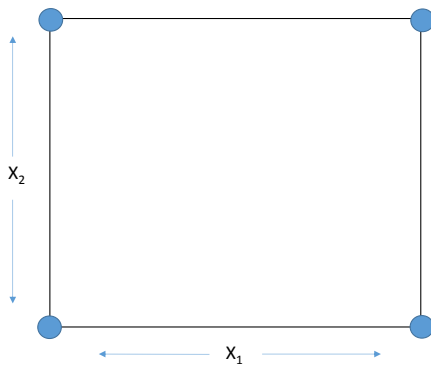


Figure 2.1 – 2 levels 2 factors design

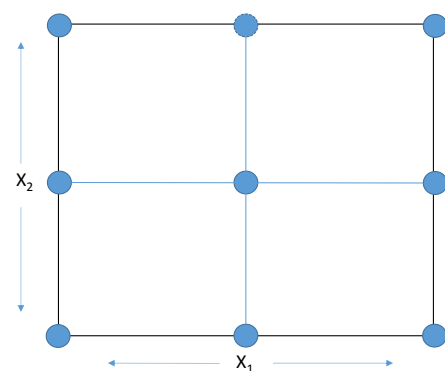


Figure 2.2 – 3 levels 2 factors design

For a three level experiment, additional five runs are needed, as Figure 2.2 shows. The required number of runs increases dramatically, as Table 2.1 on the next page shows, with the increase of factors (k) and levels (N).

Number of runs = k^N			
$k \backslash N$	2	3	4
2	4	8	16
3	9	27	81
4	16	64	256
5	25	125	625
6	36	216	1296

Table 2.1 – Full factorial runs

For small number of factors and levels, the number of runs is feasible. When dealing with multiple factors, the large amount of required runs for full factorial design makes the experiment very time-consuming. The full factorial central composite design play an important role in response surface methodology (Myers et al., 2011).

2.1.2. Central Composite Design (CCD)

CCD is a design that effectively estimates the coefficients of a second-order regression function. The goal of the design is to estimate a good second-order linear regression function, with as few runs as possible and smallest variance.

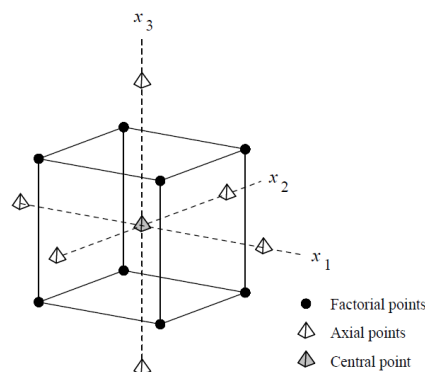


Figure 2.3 - CCD for three factors

The CCD design in Figure 2.3 consists of eight ($=2^k$) factorial points, six ($=2k$) axial points and one centre point. The number of centre point may vary, but Table 2.2 illustrates some of the standard configurations of CCD for different number of factors. In CCD, the units of each factor are converted to coded units, ranging from -1 to +1.

All the factorial points are a combination of the border of this range; (+1,+1,-1) or (-1,+1,-1) etc. for the design in Figure 2.3. The centre points are in (0,0,0). The axial points are defined by alpha (α) and for Figure 2.3 they are ($\pm\alpha,0,0$), ($0,\pm\alpha,0$) and ($0,0,\pm\alpha$).

Full factorial CCD				
k	2^k	2k	Centre points	Total Runs
2	4	4	5	13
3	8	6	6	20
4	16	8	7	31
5	32	10	10	52
6	64	12	14	90

Table 2.2 – CCD runs

The numbers of runs for the same number of factors in Table 2.2 are less than for Table 2.1. This saves time when screening an experiment.

2.1.3. Choice of α

The α -value determines how far out the axial points will be. There are two common ways to determine the value, one for spherical design and another for rotatable design.

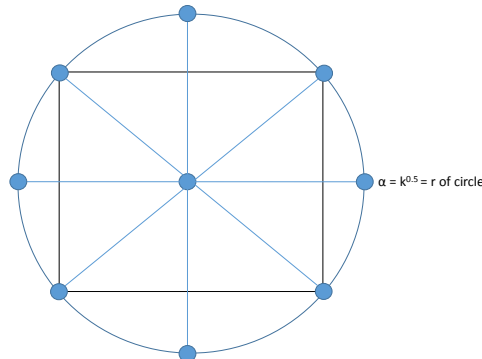


Figure 2.4 – Spherical Design

Figure 2.4 illustrate spherical design where all measured points are of equal distance to the centre point. In this way, the design is rotatable, but that is not what is meant when a design is described as rotatable. A full factorial central composite design is rotatable if

$$\alpha = 2^{\frac{k}{4}} \quad (8)$$

where k is the number of factors (Box et al., 1978). When this alpha-value is chosen, the variance is equal for all points that are at equal distance from the centre. The alpha-value is generally specified in this way.

2.2. Regression analysis

Regression analysis is a statistical method to fit a model that describes the relationship between variables. These models are empirical and are assumed valid only within the investigated range of the variables. What needs to be echoed throughout the analysis is the quote from George E.P. Box (Box and Draper, 1987):

All models are wrong, but some are useful.

This section will focus on the underlying assumptions and verification of model accuracy. Basic theory can be found in (Montgomery et al., 2012), but it is not emphasized in this report.

2.2.1. The regression function

Second-order linear regression is performed to obtain a model based on the results from the central composite design. The second-order regression function for two factors can be expressed as

$$y = \beta_0 + \beta_1 X_1 + \beta_2 X_2 + \beta_{12} X_1 X_2 + \beta_{11} X_1^2 + \beta_{22} X_2^2 + \varepsilon \quad (9)$$

The term “ y ” on the left hand side is the response or the dependent variable. On the right hand side are the factors or regressors (X_1 and X_2) and their coefficients (β_0, β_1 etc.). The factors are considered independent from each other, and their contribution on the dependent variable can be identified. The last term is called the statistical error. This term describes the unavoidable uncertainty of empirical data and is necessary, as the model cannot fit all points perfectly. It is the error between the observed value and the “true” unobserved mean.

In this report, a software called Minitab calculates the model based on measured results. Table 2.3 illustrate a result from a full quadratic regression analysis of a CCD, performed by Minitab. The terms in the first column are all combinations of the four factors lambda (X1), H2 fraction (X2), Ratio (X3) and Distance (X4).

Coded Units				
Term	Coef	SE Coef	T	P
Constant	36,8505	0,20323	181,324	0,000
Lambda	-0,2553	0,08297	-3,077	0,009
H2 fraction	1,4894	0,08297	17,951	0,000
Ratio	-0,0661	0,08297	-0,797	0,440
Distance	0,2478	0,08297	2,987	0,010
Lambda*Lambda	-0,1930	0,08297	-2,326	0,037
H2 fraction*H2 fraction	-0,2437	0,08297	-2,938	0,012
Ratio*Ratio	-0,1161	0,08297	-1,399	0,185
Distance*Distance	0,0829	0,08297	0,999	0,336
Lambda*H2 fraction	0,3180	0,10161	3,130	0,008
Lambda*Ratio	0,1169	0,10161	1,151	0,271
Lambda*Distance	-0,0857	0,10161	-0,844	0,414
H2 fraction*Ratio	0,0506	0,10161	0,498	0,627
H2 fraction*Distance	-0,1138	0,10161	-1,120	0,283
Ratio*Distance	-0,1389	0,10161	-1,367	0,195

S = 0,406459 PRESS = 9,57010
R-Sq = 96,63% R-Sq(pred) = 84,99% R-Sq(adj) = 93,01%

Table 2.3 – Full quadratic model example

The second column lists the corresponding coefficients of the terms (β_0, β_1 etc.). The next column is the standard error of the coefficient of each term. The p-values listed at the end are the probability that the term is not relevant to the function. If this value is outside the confidence interval, the term is not statistically significant. It means that the observed influence of this term can be of mere chance. The analysis is performed in coded values. The terms are independent of each other, so any term may be deleted to improve the model.

2.2.2. Assumptions for linear regression

From (Montgomery et al., 2012) the major assumptions of regression analysis are:

1. The relationship between the response y and the regressors is linear, at least approximately.
2. The error term e has zero mean.
3. The error term e has constant variance s^2 .
4. The errors are uncorrelated.
5. The errors are normally distributed.

The error term referred to in the assumptions is the same defined in equation (9). It is often confused with the residual which is defined as (Montgomery et al., 2012):

$$e_i = y_i - \hat{y}_i, i = 1, 2, 3 \dots n \tag{10}$$

The error (e) is the difference between the observed value (y) and the fitted value or value the model describes (\hat{y}). These residuals are however very helpful to test the model for the given assumptions.

2.2.3. Residual plots

The residuals describe the difference between the observed value and the model. Plotting these in different ways can help indicate any departures from the assumptions in section 2.2.2. The example in Table 2.3 gave following residual plots in Minitab.

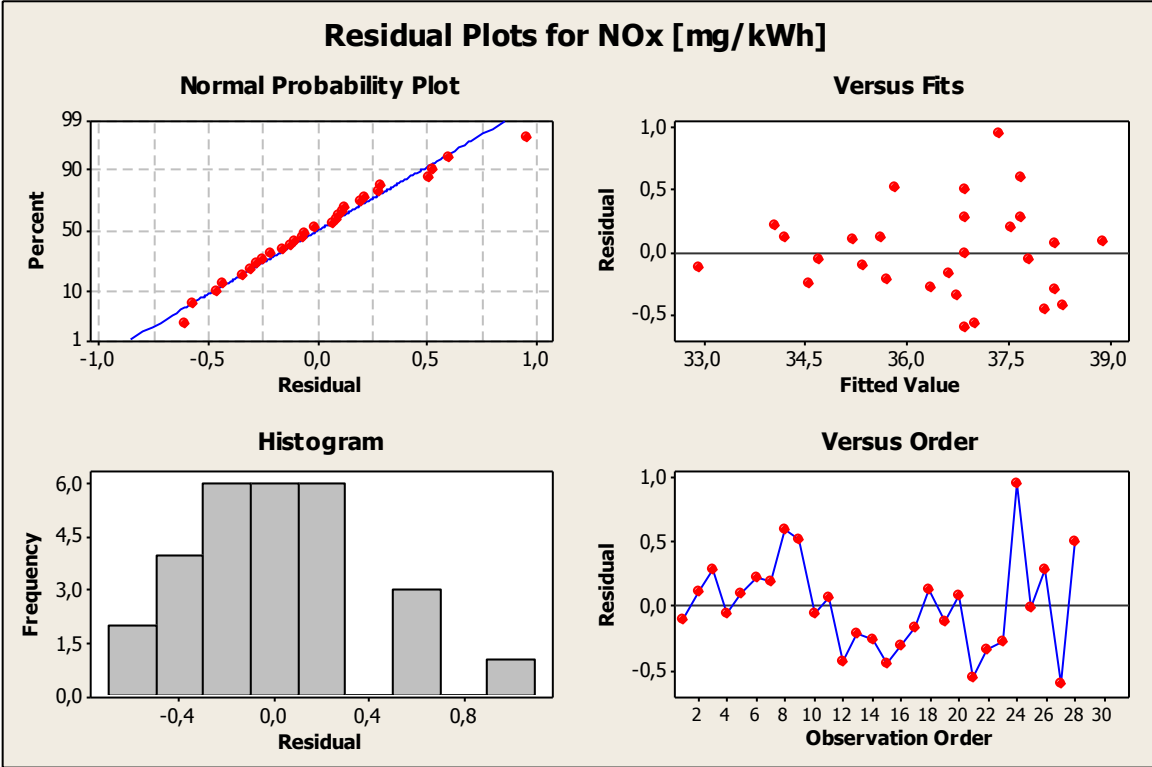


Figure 2.5 - Residual Plots Example

The graph at the bottom right in Figure 2.5 illustrates how the residual changed over time. If, for example increasing, the residual along the observation increased steadily, it may indicate that the measurements are influenced by some unexplained variable over time. It could be that the measurement device’s accuracy slides out with time and should be calibrated more often. The top right graph should display a random cluster of points over the fitted values.

Systematic trends in the residuals over the fitted values are an indication of a badly fitted model. It could be the case that a first-order model is fitted to a relationship that actually is of second-order, a missing variable or term. The top left graph illustrate if the residuals are normally distributed. They should be, and the graph describes any departures from this. The histogram will indicate any outliers. Outliers are observations with unusual high residual. If the cause of the outlier is found to be for example a malfunction in the measurement device, it may be removed. Removing outliers without the knowledge of the cause is not recommended. Global statistical numbers should be revised now that the model adequately meets the given assumptions.

2.2.4. R²-values and lack-of-fit test

The R²-value is explained as the percentage of the variation of observed values in the model that are explained by its relationship to the factors (Montgomery et al., 2012). In other words, how well the model fits the observed values. The predicted R²-value describes how well the model can predict a certain point within the model, based on the other observed points. If a model has a high R²-value, but very low predicted R²-value, it indicates that the model is over-fitted. The model fits the data collected very well, but is not able to predict any values in between the observed points. This type of model is not satisfactory and should be avoided. To improve the model, statistically insignificant terms can be removed. It might be necessary to run another experiment with factors with different ranges. The adjusted R²-value takes into account the number of observations in the model. In addition to these key-values, the lack-of-fit test should also be evaluated. If the p-value of the lack-of-fit test is less than the α -level (0.05), the model does not, within a confidence of 95 %, fit the observed values. A model of higher order, logarithmic scale or similar may be necessary to describe the observed values better. For higher p-values of the lack-of-fit test, this cannot be stated.

2.2.5. Modelling

There are many things to take into account when presenting a model. Iterative improvements based on analysis, reflection and carefulness are perhaps the best way to obtain a good model that represents the empirical data.

3. Theory of errors

3.1. Introduction

Many things can go wrong during an experiment. For the outcome to be trusted, a thorough investigation of errors and deviations is crucial. There will always be random uncertainties in all types of measurements. However, systematic errors can affect the results and are not as easy to detect. These occurrences should be in mind when planning, conducting and analysing an experiment.

3.2. Types of errors

In general, errors are categorised into three types:

- i. Human error
- ii. Systematic deviation
- iii. Uncertainties

The first type of error should be avoided completely, but can be hard to realise. Human error can be of stupidity, accidental or intended. Intended human errors should never occur, as this is considered as a fraud. With experience of conducting the experiment, stupid errors should eventually not be present and accidental errors avoided by well-defined methodology executed to the point.

3.2.1. Systematic error

Consistent deviation is observed when for example some instrument is not calibrated correctly. This systematic error will propagate itself in all the results measured by the incorrect setup. Errors like this are hard to pinpoint, as the result may seem reasonable if two errors pull in different directions. Thorough tests to make sure all apparatus work as desired should be conducted. The more instruments a result is dependent on, the harder it is to locate where a potential deviation is originated. Therefore, it is important that all instruments are calibrated correctly so that the real and actual value is measured and logged. Results should be checked against theoretical values at all possible stages of the experiment.

3.2.2. Uncertainties and random error

All instruments, even when calibrated correctly, have a degree of uncertainty. This is provided by the manufacturer in the manual or data sheet, and should be taken into account when presenting the results. Because this error occurs

randomly, it should be described statistically. If an apparatus has an error of one percent of its full range, this will define the standard deviation of the measurement. For all parameters in an experiment, these deviations should be taken into account and summed up to describe the deviation in the result.

3.3. Propagation of errors

The result's precision is always described as a function of one or more parameters. Each measurement or reading includes an uncertainty. In order to propagate the error through the function correctly, it must be determined if the parameters are independent of each other. An arbitrary example is given by a response ($f(x)$) that is defined as three times the measured parameter (x):

$$f(x) = 3(x \pm 0.01) \quad (11)$$

then it follows that (Berendsen, 2011):

$$\sigma_{f(x)} = \left| \frac{\partial f(x)}{\partial x} \right| \sigma_x = 3\sigma_x = 0.03 \quad (12)$$

The deviation of the result will be three times of the measured parameter (+/- 0.03). However, the errors have to be added up differently if the result is a function of multiple independent variables. Since the parameters may deviate in positive and negative direction, they often seem to cancel each other out, to a certain degree. The appropriate way to calculate the standard deviation of a result is to take the square root of the sum of the squared errors of each parameter (Berendsen, 2011):

$$\sigma_{f(x,y,\dots,n)} = \sqrt{\left(\frac{\partial f(x,y,\dots,n)}{\partial x} \sigma_x \right)^2 + \left(\frac{\partial f(x,y,\dots,n)}{\partial y} \sigma_y \right)^2 + \dots + \left(\frac{\partial f(x,y,\dots,n)}{\partial n} \sigma_n \right)^2} \quad (13)$$

4. Method of measurement

4.1. Equipment

4.1.1. Mass Flow controllers

Mass flow controllers						
Alicat	Gas	Range	Model	Serial	STP	Error
MFC 51	H ₂ P	300	MC-300NLPM-D	45257	0°C, 1 atm	0.8% of Reading + 0.2% of Full Scale
MFC 47	CH ₄ P	150	MC-150NLPM-D	37923	0°C, 1 atm	0.8% of Reading + 0.2% of Full Scale
MFC 48	CH ₄ S	100	MC-100NLPM-D	40019	0°C, 1 atm	0.8% of Reading + 0.2% of Full Scale
Brooks	Gas	Range	Model	S/N	STP	Error
MFC 16	H ₂ S	100	5851	T80397/003	0°C, 1 atm	1% of Full Scale
MFC 17	Air	900	563S	T80397/001	0°C, 1 atm	1% of Full Scale

Table 4.1 – Mass Flow Controllers

Range is given in normal litres per minutes. In order to minimise the error, the mass flow controllers were chosen to match the ranges they were likely to operate. After all controllers were installed, a pressure test was conducted over night. The system passed when only minimal reduction of pressured was measured. The controllers were then tested against a calibrator, as described in the section of investigation of errors (5.2.3).

4.1.2. Gas analysers



Figure 4.1 – Gasetm DX4000

The Gasetm™ DX4000 (yellow box) measures the exhaust gas directly without condensing out any water first. It is based on Fourier transfer infrared spectroscopy (Gasetm). The oxygen is measured by the portable sampling unit that also control the heated pipes. The sampling unit is calibrated for oxygen with the ambient air, while the DX4000 is calibrated only by zero gas (N₂).



Figure 4.2 - HORIBA PG-250A

The HORIBA PG-250A (HGS No. PGEK03NC) was used to measure NO_x in this report. Since the PG-250 cannot handle more than 20% water in the flue gas, the sample gas went through a cooler first. The analyser uses chemiluminescence to measure NO_x and has an expected error of $\pm 1\%$ of full scale (100 ppm).

4.1.3. Temperature Probes

Three probes were installed. It was not of great importance to verify the accuracy of these values as they were only used as indicators. The probes measured temperatures of:

- 1) Outer chamber wall (T2)
- 2) Air by inlet (T4)
- 3) Fuel at collector (T1)
- 4) Exhaust gas (T3)

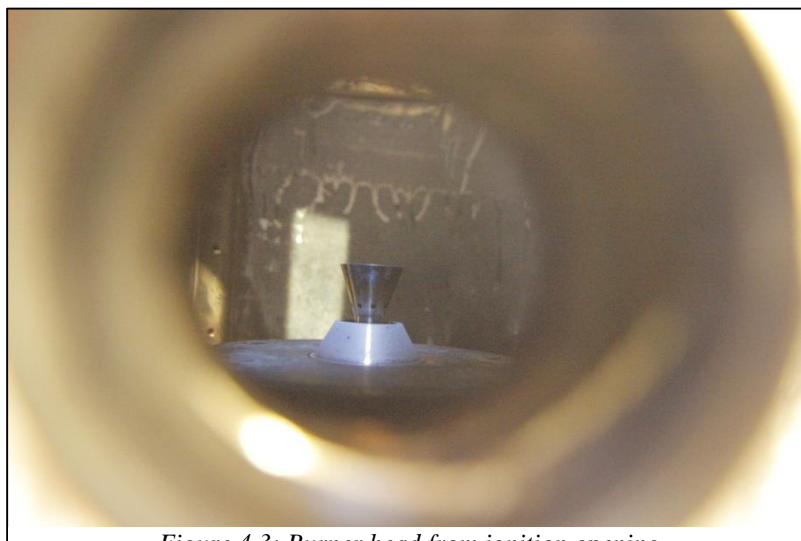


Figure 4.3: Burner head from ignition opening

4.2. Setup

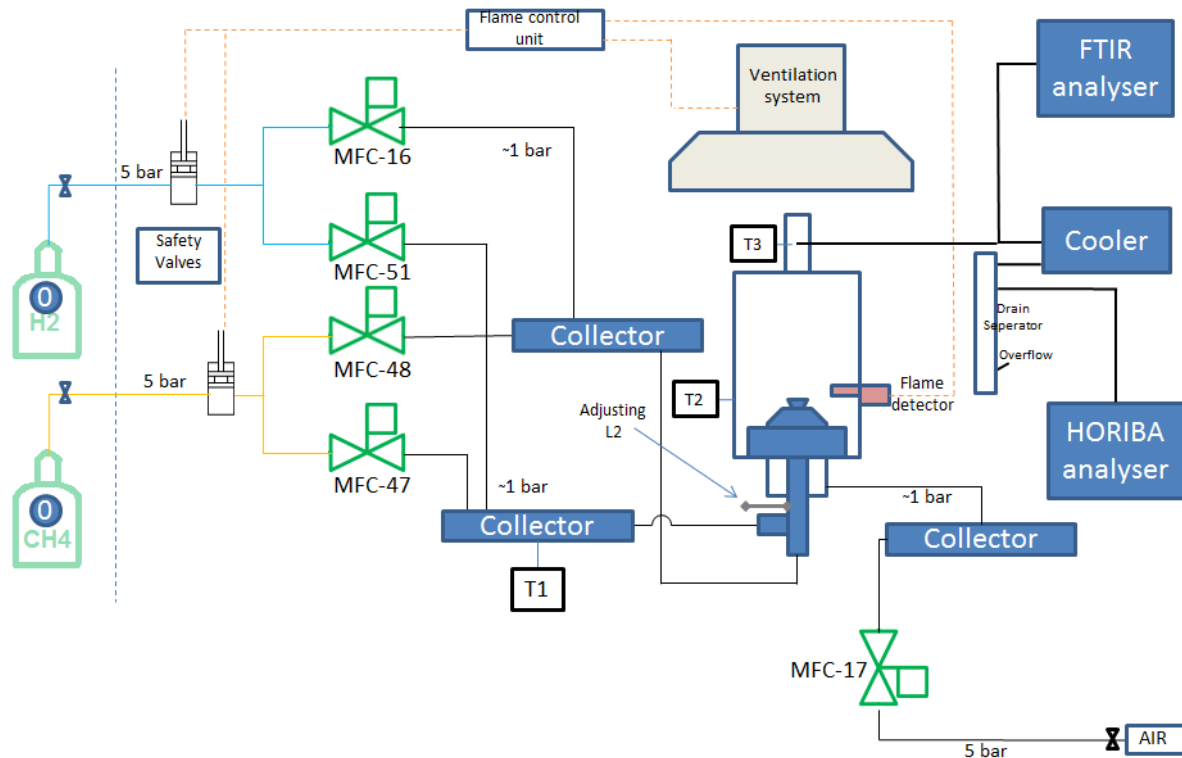


Figure 4.4 – Configuration of the test rig

The pipe flow system has two main safety valves between the MFCs and the gas bottles containing hydrogen and methane. These valves must have an electric current to stay open. The current was cut by the flame control unit in case of emergencies (autonomous shutdown), blow out in the burner, no suction at the roof fan and by pressing the stop button. The fuels are mixed in two collectors, one for primary fuel and one for secondary, before entering the burner.

Compressed air was provided from the wall and was fed in parallel to the three MFCs at five bars. The three flows were mixed in the third collector and fed into the burner. The flame detector was installed to close the safety valves on the fuel lines if the flame blew out. Adjustment of the length L2 were done manually with a wrench underneath the burner. The gas bottles and the air feed were opened to a pressure of five bars. All mass flow controllers, temperature sensors (T1, T2, T3 and T4), results from the HORIBA gas analyser were controlled and logged in Labview.

The mass flow controllers from BROOKS use correction factors on the flow rate for the calibration gas to calculate settings needed to obtain correct mass flow rate of other gases. The MFCs from Alicat has this function implemented.

Sample of the flue gas was sucked out from the cylindrical nozzle at the top of the chamber. The smaller diameter ensured turbulence and fully mixed sample. In the first test, the probe was installed further down. It was then observed differences in measurement when adjusting the probe's position radially. This was not the case when the probe was at the nozzle. The sample gas was split in two. One to the FTIR gas analyser and the other to the cooler and then the HORIBA gas analyser.



Figure 4.5 – Overview of the rig

4.3. Procedure

The gas analysers were always calibrated in the morning, before start up. After warming up for an hour, the zero and span points was set by high quality calibration gas for CO, CO₂, and NO. The FTIR-analyser was purged with N₂ and then calibrated for O₂ with the ambient air. These procedures are necessary, but time consuming. In order to skip the warm up time of one hour, the HORIBA gas analyser was sometimes not turned off after purging at the end of the day. In that way, one could calibrate it straight away. The roof fan in the

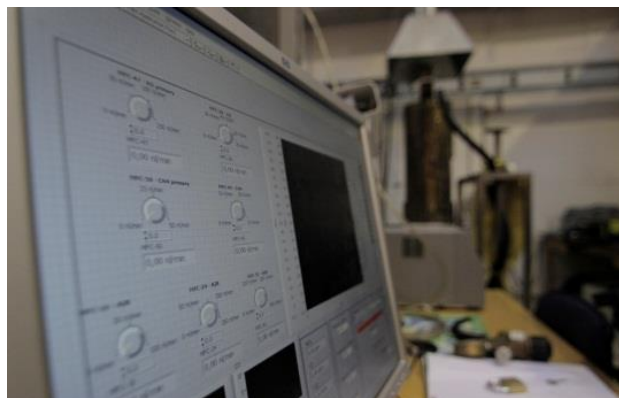


Figure 4.6 - Control Panel (LabView)

laboratory was turned on so that there was suction at the outlet. Labview was started, the air opened to five bar and the mass flow controllers was opened to flush the chamber with air for a couple of minutes. The water cooling system was turned on. The pipe between the safety valve and MFC was pressurised with five bars of gaseous fuel. The burning was then initiated by opening the MFC for methane, while the correct amount of air already flow into the chamber, and pressing the green start button on the electrical cupboard. The power was set to 3 kW and was ignited with a gas torch through a hole at the side of the chamber. The measurements were logged for a couple of minutes, then averaged and compared to theoretical values for a quick verification. When stopping the burning, the red stop button was pressed and the chamber was flushed with air for a couple of minutes. A more detailed documentation of the HSE procedures is attached in the appendix.

5. Investigation of errors

5.1. Human errors

5.1.1. Configuration of sampling gas

The measured values of carbon dioxide and oxygen in the gas analysers were always different from the theoretical values calculated. These consistent deviations in the result led to a series of investigations on all parts of the rig, between experiments. Several improvements in the configuration of the rig was the result of these investigations.

Initially, the gas was extracted from the probe to the drain separator, then to the remote cooler that pumped sample gas to the HORIBA gas analyser. The high velocity of the sample gas from the cooler resulted in an overflow to the gas analyser and insufficient condensation of the sample gas in the cooler. Hence, too much and too wet sample gas was provided to the gas analyser, which may cause wrong results and even damage the instrument. Firstly, the believed reason for this was a choked filter prohibiting the water to be drained from the condenser. The filter was changed, but the same happened again. The water pump inside the cooler was checked; it was broken and needed new parts. Now that the draining of the condenser worked, but water still came up through gas outlet of the cooler. Too high flow rate forcing water up into to gas pump was thought to be the cause. The drain separator was installed between the cooler and the gas analyser instead. In this configuration, the drain separator played a

different role as a valve that disposed the overflow of sample gas that the gas analyser did not suck. The flow of sample gas from the cooler could then be adjusted to the gas analyser's need and minimise the flow rate. Finally, the configuration worked properly; water was extracted in the cooler and the gas analyser operated with correct flow rate.

Every time something was fixed and the cooler was believed to be working, water came out the gas outlet after some time of measuring hot and wet exhaust gas. Hence, the problem consumed a lot of time and ruined many results.

5.2. Systematic deviations

5.2.1. Leakage diluting gas samples

Despite the configuration working properly, the deviation in carbon dioxide and oxygen levels were still observed. Because the ratio of carbon dioxide and oxygen did not correspond, a leakage after combustion was suspected. The downside of the cooler, between the cooler and the probe into the chimney, is under-pressurised due to suction from the pump. Leakages from the ambient, diluting the sample gas, was therefore possible. By providing pure nitrogen gas to the probe, it would be possible to detect any leakage if oxygen was measured. There was zero amount of oxygen, indicating that everything was well sealed. However, the nitrogen was provided at higher pressure than the ambient causing the leakage to inverse or at least stop any ambient air into the sample gas. When nitrogen then was provided at ambient pressure, using the drain separator, oxygen was measured. All connections were thoroughly checked again and sealed until the pipe system passed the test. The leakage test for the pipe system was after this conducted before and after all measurements.

5.2.2. Real flow from MFCs

Systematic deviation due to the leakage was eliminated. Both gas analysers measured the same values, unlike before. However, a deviation in the values was still observed. Confident that the gas analysers now measured real values, assuming full combustion, the mass flow controllers were investigated closer. It was possible the actual flows of methane, hydrogen and air into the chamber were different from what was set in Labview. When comparing the set point in Labview and the logged flow from the MFCs, following results were observed:

Fuel Ratio [Log/Set]				
CH4 P	CH4 S	Air	H2 S	H2 P
0,93	0,97	1,00	1,0	1,0
0,91	0,94	1,00	1,0	1,0
0,93	0,94	1,00	1,0	1,0
0,91	0,97	1,00	1,0	1,0
0,92	1,00	1,00	1,0	1,0
0,90	0,99	1,00	1,0	1,0
0,93	0,99	1,00	1,0	1,0
0,90	0,95	1,00	1,0	1,0
0,93	0,96	1,00	1,0	1,0
0,89	0,92	1,00	1,0	1,0
0,91	1,00	1,00	1,0	1,0
0,91	1,01	1,00	1,0	1,0
0,93	-	1,00	1,0	1,0
0,91	0,99	1,00	1,0	1,0
0,91	0,99	1,00	1,0	1,0
0,92	1,03	1,00	1,0	1,0
0,92	0,98	1,00	1,0	1,0
0,92	1,00	1,00	1,0	1,0
0,92	0,96	1,00	1,0	1,0
0,92	0,91	1,00	1,0	1,0
Average difference in percentage				
91,64	97,35	100,00	100,00	101,11

Table 5.1 – Fuel difference

Table 5.1 shows a consistent difference in the flow of methane through the mass flow controllers (MFCs). All though the difference in methane through secondary holes is smaller, the value of flow compared to the range of the mass flow controller is low, thus high uncertainty, and makes these measurements unreliable in this case. For methane that is provided to the primary holes, or MFC-47, the uncertainty is smaller and the logged value is on average 91.64% of the set value in Labview. If assuming ideal gas, constant pressure and mass flow:

$$\frac{V_1}{V_2} = \frac{T_1}{T_2} \quad (14)$$

Any difference in temperature is equal to the difference in volume. When the value in Labview is set, it is in normal litres (0°C, 1 atm). The MFCs from Alicat, however, are calibrated for normal litres (25°C, 1 atm) (Alicat). The ratio is then:

$$\frac{273,15}{298,15} = 0,9161 = 91,61\% \quad (15)$$

There is a clear correlation of this ratio and the ratio between Labview and the logged value of methane for MFC-47. However, there is no evidence for which of the two quantities of mass flow rate that actually is provided to the chamber. In order to investigate this, an independent test is necessary.

5.2.3. Calibration of MFC

All the mass flow controllers on the rig were tested against a high precision calibrator. The calibrator's uncertainty is very low and is calibrated itself regularly by the manufacturer. In other words, the device is used as set answer. Air was provided at five bars to the mass flow controllers. The calibrator was connected downstream of the controllers, measuring the flow. The whole range of the MFCs were tested with intervals of 0, 25, 50, 75 and 100% and repeated five times. The set point in Labview was noted, as well as the reading from the calibrator after steady state was reached. Following results were obtained:

The errors presented in Table 5.2 did not vary much over the flow range of the MFCs as can be studied closer in the appendix E. On average, the actual flow of air through MFC-47 was 0.74% above the set point in Labview. It suggests that the value set in Labview is the actual value of the flow into chamber, not the value logged from the mass flow controller, as previously discussed. In MFCs from Alicat, the desired type of gas is simply chosen in its panel and the MFC

Flow test of MFCs	
Instrument	Overall averaged error [%]
MFC-17 (Air)	-0,36
MFC-16 (H2 S)	1,36
MFC-51 (H2 P)	2,20
MFC-47 (CH4 P)	0,74
MFC-48 (CH4 S)	0,42

Table 5.2 – Calibration of MFCs

corrects the flow. Deeper investigation of the electrical current signal, or how the signal from Labview is processed before returning, has not been carried out, and may be a source of error. These issues should be investigated further for future measurement campaigns. The difference in NO_x [mg/kWh] due to the uncertainty of how much fuel is provided is anyway within the standard deviation. The gas analyser is the larger source of pure error. The results in Table 5.2 have not been taken into account. The measurements are only for qualitative study.

5.2.4. Factors of short ranges

In the design of some of the experiments, the ranges of the physical factor like R2 and L2 were compromised in order to obtain full combustion. The amount of fuel that was provided to the secondary holes was around one percent of the range of mass flow controllers. When operating at these low values, the uncertainties of flow almost exceeds the value itself. The relative error of the device becomes very large, but the absolute error is still small compared to the total flow of fuel when taking into account the primary holes. This way, the

measurement of NO_x is not affected to any significant degree. However, the actual flow of fuel to the secondary holes, thus exactly what point the burner operates, is uncertain. In other words, it will be impossible to determine any statistical trends for that specific factor. This problem is observed for all experiments, except the last one. Due to constant presence of hydrogen, the range of R2 and L2 could be increased and information of their influence on NO_x emission could be documented. This is supported in the results and will be discussed later.

5.2.5. Summary

Due to leakages and gas analysers not operating at normal conditions the results for the first matrix for both the methane and hydrogen lance, cannot be justified quantitatively. However, the experiment only aims to investigate trends and the errors are systematic deviation throughout all the points. As discussed, the range of R2 in the first matrix is too little to give any statistical significant results. In reality, only three factors were tested.

After fixing multiple problems in the lab, the results came closer to expected values, but still, there were observed some systematic deviations. These systematic errors, however, were insignificant enough compared to error from measuring NO_x with the gas analyser and therefore ignored.

The standard deviation for each measurement of NO_x is expressed in the results.

6. Results

The results are presented in the order of importance where the most precise and reliable measurements are presented first.

6.1. The hydrogen lance

6.1.1. 2nd Matrix

The hydrogen lance was first tested to map the boundaries of which it could operate. The ranges of each factor were, based on these tests, chosen as wide as possible. Table 6.1 displays the factors and ranges tested in this experiment.

Factor	Unit	Coded units				
		- α	-1	0	1	+ α
R2	%	0	4,1	10	15,9	20
L2	mm	13	14,4	16,5	18,6	20
H2	wt%	5	10,1	17,5	24,9	30

Table 6.1 – Table of factors, 2nd Matrix

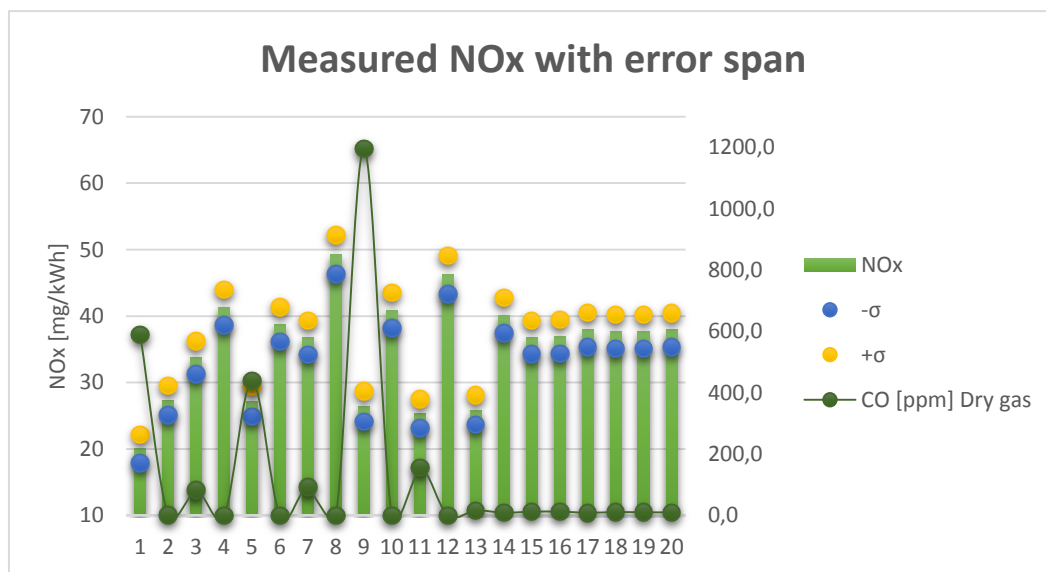


Figure 6.1 – NOx response for 2nd Matrix

The burner was set to operate at 15kW (LHV) and an equivalence ratio of 1.14 for all measurement points. The intention for this experiment was to investigate how the settings of the physical factors of the burner, namely height of lance distance and amount of fuel to secondary holes, affected the production of NOx during combustion in more detail. The matrix consisted of 20 points and the amount of NOx measured for each point is presented in Figure 6.1.

The responses of NOx measured were diverse. The standard deviation of the measurement is around 2.8 mg/kWh for all measurements and is considerably

less than the variations of emissions for the different points. Differentiating the random error from the actual difference between the measured points is crucial to obtain a statistical robust model. It is worth mentioning that full combustion was not obtained for some of the points. The model however is based on the assumption of full combustion.

A statistical model is obtain by analysing the data in Minitab. The full quadratic regression analysis gave the following results.

Coded Units					
Term	Coef	SE Coef	T	P	
Constant	40,3726	0,2764	146,081	0,000	
%H2	5,0490	0,1834	27,535	0,000	
L2	6,5361	0,1834	35,645	0,000	
R2	4,2462	0,1834	23,157	0,000	
%H2*%H2	-1,3365	0,1785	-7,488	0,000	
L2*L2	-0,6048	0,1785	-3,388	0,007	
R2*R2	-1,7174	0,1785	-9,621	0,000	
%H2*L2	0,1844	0,2396	0,770	0,459	
%H2*R2	1,2250	0,2396	5,113	0,000	
L2*R2	-1,0378	0,2396	-4,332	0,001	

S = 0,677634 PRESS = 24,0512
R-Sq = 99,64% R-Sq(pred) = 98,10% R-Sq(adj) = 99,31%

Table 6.2 - Full quadratic model of 2nd Matr Hydrogen Lance

As Table 6.2 shows, all terms of the full quadratic function have very low probability (p-value) of not being relevant for the regression function, except for the two-way interaction of H2 and L2. It is 45.9 percent likely that relationship the term describes, with its coefficient, was observed by chance. The coefficient of the term is not significant, as Figure 6.2 illustrates.

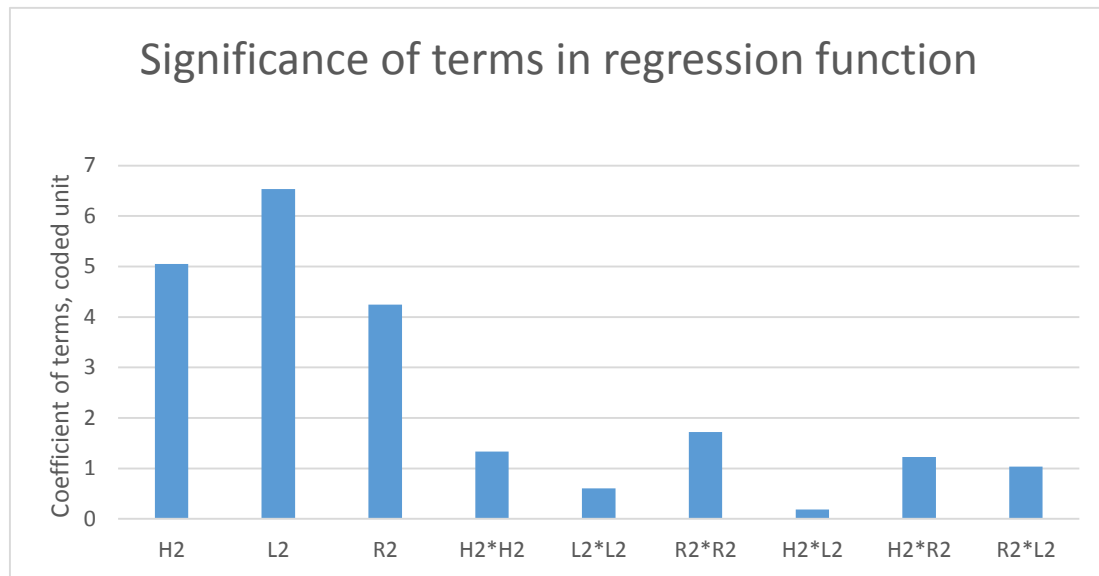


Figure 6.2 – Coded significance of terms

The term H2 times L2 was removed from the model. The remaining terms still give a very precise model. The low p-values for the rest of the terms indicate a good model is obtained.

$$NOx = -0.024X_1^2 - 0.140X_2^2 - 0.049X_1^2 + 0.028X_1X_3 - 0.084X_2X_3 + 1.249X_1 + 8.587X_2 + 2.587X_3 - 89.748 \quad (16)$$

Coded Units					
Term	Coef	SE Coef	T	P	
Constant	40,3726	0,2712	148,863	0,000	
%H2	5,0490	0,1799	28,059	0,000	
L2	6,5361	0,1799	36,324	0,000	
R2	4,2462	0,1799	23,598	0,000	
%H2*%H2	-1,3365	0,1752	-7,630	0,000	
L2*L2	-0,6048	0,1752	-3,453	0,005	
R2*R2	-1,7174	0,1752	-9,805	0,000	
%H2*R2	1,2250	0,2351	5,210	0,000	
L2*R2	-1,0378	0,2351	-4,414	0,001	

S = 0,664970 PRESS = 20,2148
R-Sq = 99,62% R-Sq(pred) = 98,40% R-Sq(adj) = 99,34%

Table 6.3 – Final model for 2nd Matrix, Hydrogen Lance

The regression function (16) is in uncoded units, meaning the amount of NOx is in milligrams per kilowatt-hour and the three factors correspond to its original unit as stated in Table 6.1. The high value of R² in Table 6.3 states that the model fit the observations very well. Predicted R² is very close to 100% and states that the model is able to predict response values of NOx, within the defined ranges of the factors, very well. This indicates that the model is not

over-fitted to match only the observed values, but fits all other combination of the factors.

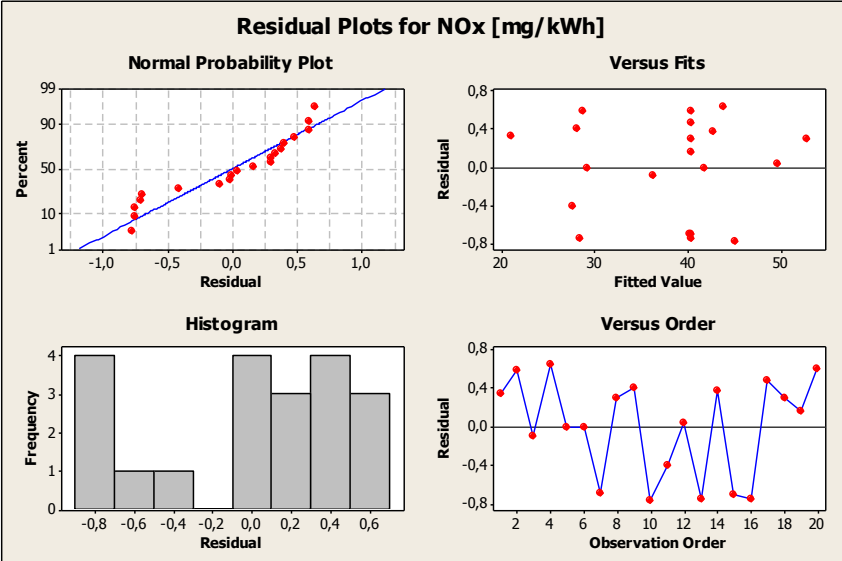


Figure 6.3 - Residual Plots, 2nd Matrix, Hydrogen Lance

The residual plots in Figure 6.3 give rise to some issues. The bottom right graph indicates that the residuals are random spread around zero over time. The histogram detects some outliers some degree and the normal probability plot shows a clear S-curve along the residuals. Lastly, the top right graph illustrate that the residuals are even spread around zero, but not as random. The points seem to be clusters in some fitted values. A fourth factor or variable can be the cause of these irregularities and the presence of CO for some measurement points are investigated closer.

The model is able to describe how the three factors affect the emission of NOx, independently. Unable to present the results in three dimensions, the third factor is held constant. Of course, the graph will be change for different hold values and must be kept in mind when analysing the results.

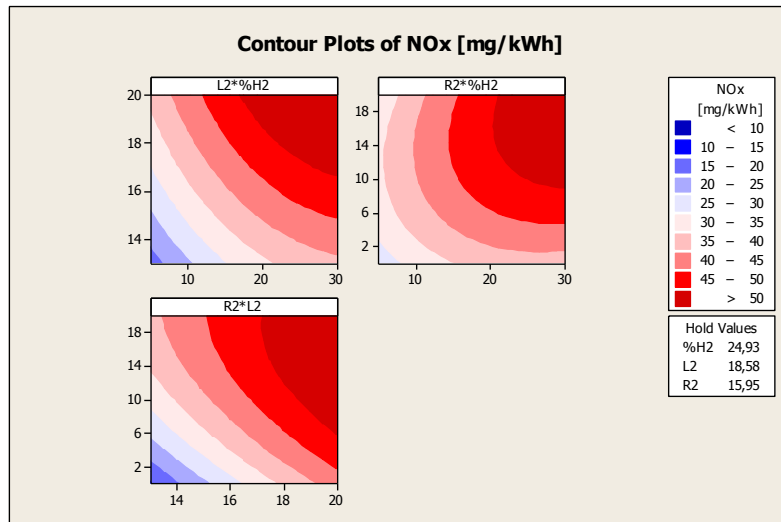


Figure 6.4 – High Hold values, 2nd Matrix Hydrogen Lance

Figure 6.4 show the results when the factors are held constant at high values i.e. the interaction between R2 and L2 is displayed when the fuel consists of 24.93 percent of hydrogen.

It is clear from Figure 6.4 that hydrogen contributes to increased emission of NO_x. If the fuel is distributed to the secondary holes of the burner, the emission will increase, especially for higher values of hydrogen in the fuel. This increase can be observed for all distances of L2. It suggests that the optimal setting for the burner has no fuel distributed to the secondary holes. When 15.95 percent of the fuel goes to secondary holes, lower lance position (L2) will decrease the emission as well as dampen the increase of emission when hydrogen is added. This effect was observed for all values of R2. It suggests that the optimal setting for the burner has a low value of L2.

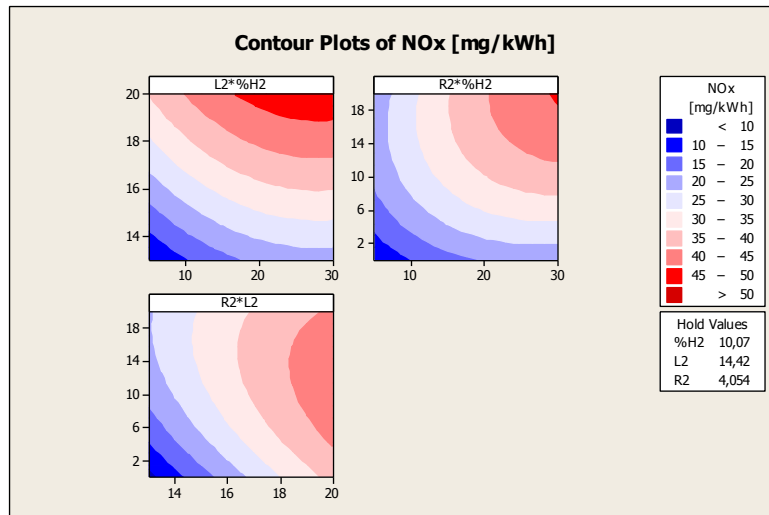


Figure 6.5 - Low Hold Values, 2nd Matrix Hydrogen Lance

Figure 6.5 shows considerably lower levels of emission than Figure 6.4. As Figure 6.4 illustrates, even low values, like 4 percent of fuel to the secondary holes, of R2 results in higher emission of NOx. The influence of R2 on the emission level, over the range of fuel compositions, has the same trend for low hold value of L2 as for high values. For low values of L2, supply of fuel to secondary holes of the burner has a stronger negative effect on the emission level. It therefore follows that the positive effect of reducing L2 is greater when R2 is held at low values, especially for hydrogen-rich fuel. From the top left graph in Figure 6.5, it is illustrated how much the position of the burner head influence the emission for all types of fuel compositions. Interestingly, the increase in emission of NOx stagnates as more hydrogen is added for constant value of L2.

As Figure 6.1 shows, it was measured carbon monoxide for some of the points. The FTIR gas analyser was able to detect the whole range of CO emissions. By implementing this data in the same design of experiment in Minitab, a response surface of CO was produced. Because the production of CO may have an exponential function, the natural logarithm of the logged values of CO were used and then calculated back after the model was analysed.

Coded Units				
Term	Coef	SE Coef	T	P
Constant	2,353	1,3067	1,801	0,092
%H2	-7,953	1,0214	-7,787	0,000
L2	-4,058	1,0214	-3,973	0,001
%H2*%H2	-2,548	0,9893	-2,576	0,021
L2*L2	-2,908	0,9893	-2,940	0,010

S = 3,77444	PRESS = 492,819
R-Sq = 85,77%	R-Sq(pred) = 67,19%
	R-Sq(adj) = 81,98%

Table 6.4 - Regression analysis for CO

Table 6.4 states that the model is not very good; prediction of unobserved values is not very accurate. A finer measurement of the region where the increase is observed is required to improve the model. The R^2 for the observed values is better so the model can give an indication for the CO production of the measured values. The third factor, R2, was not statistically significant and therefore not included in the model.

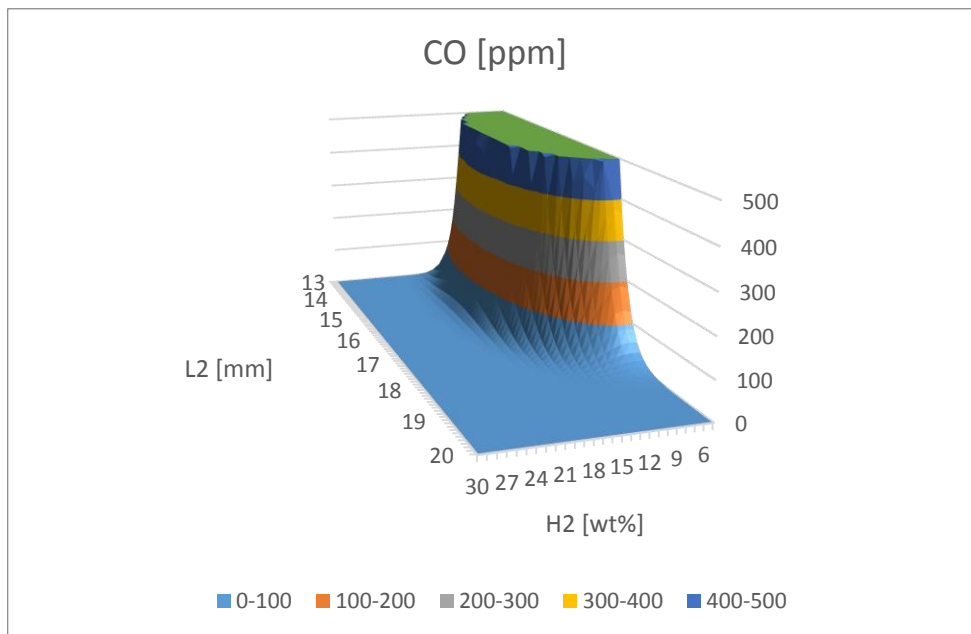


Figure 6.6 – CO levels, 2nd Matrix Hydrogen Lance

Figure 6.6 illustrates in which region concentrations of CO was observed, hence full combustion was not obtained. If both the distance L2 and the hydrogen content were under a certain threshold, there was a strong exponential growth of CO. For higher values of hydrogen-content, full combustion over the whole range of L2 was obtained. As long as the distance L2 was great enough, full combustion was obtained for the whole range of fuel compositions tested.

As mentioned, the regression analysis of the result does not describe a precise model. The exponential growth of CO, combined with the few measuring points

in the relevant region, may result in an over-fitted model. This gives room for large errors in quantitative values in that region. Even though the exact amount of CO is hard to predict in the exponential region, the region itself is nonetheless very much proven. The borders of the region may also be uncertain, but the high CO emissions when burning hydrogen-poor fuel with low distance of L2 has a clear trend.

The model states that the amount of CO is strongly dependent on the two factors H2 and L2. It also states that incomplete combustion occurs when both the burner operates at low values of these two factors, at 15 kW, for all values of R2 and 14 percent of excess air.

6.1.2. 1st Matrix

The hydrogen lance was tested for the same ranges and factors as the methane lance to obtain comparable results. Preliminary test was carried out to ensure the burner could operate within the ranges of the experiment.

Four factors were investigated; fuel composition, excess of air, burner head position L2 and the amount of fuel distribution to secondary holes. The burner operated at 25 kW. The high power ensured tolerable amounts of carbon monoxide throughout all measurements.

Factor	Unit	Coded units				
		- α	-1	0	1	+ α
λ (X1)	-	1,05	1,1125	1,175	1,2375	1,3
H2 (X2)	wt%	0	3,75	7,5	11,25	15
R2 (X3)	%	0	1,5	3	4,5	6
L2 (X4)	mm	20	21,25	22,5	23,75	25

Table 6.5 – Table of factors, 1st Matrix

As Table 6.5 shows, four factors were investigated for this experiment. It required 31 measurement points; 16 cube points, 8 axial points and seven center points. The center points were measured at random intervals during the experiment to give a likely estimate of the experimental error.

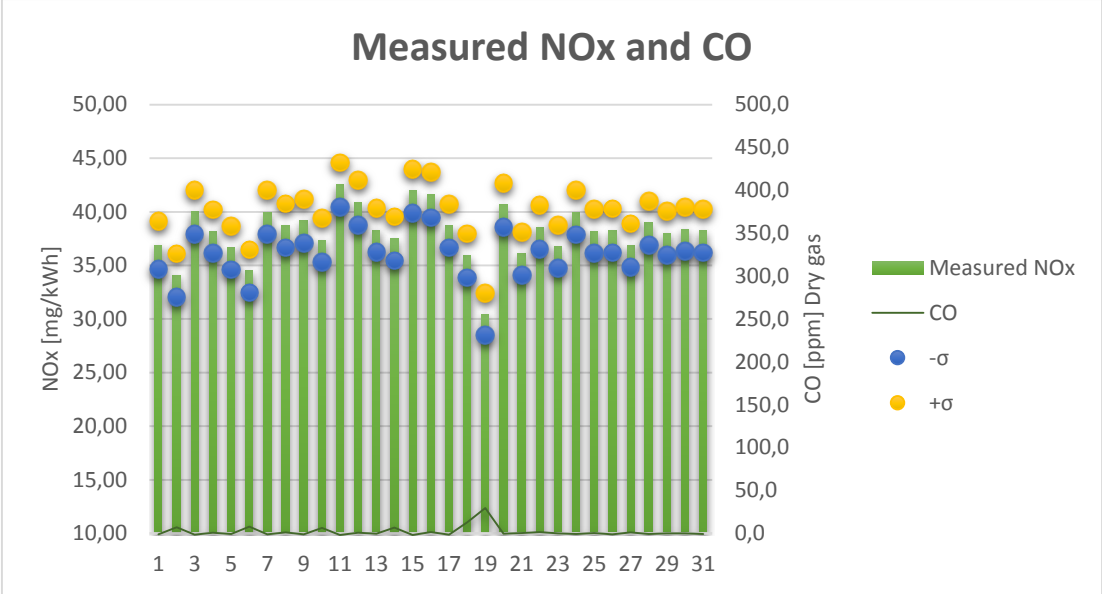


Figure 6.7 – Nox and CO, 1st Matrix Hydrogen lance

As Figure 6.7 shows, the carbon monoxide levels were considerable less for this experiment throughout all the, except point 19 perhaps. The variation of NOx levels were much less for this experiment than the previous, presented in Figure 6.1. It is obvious from Figure 6.7 that the standard deviation is rather large compared to the variation of measured values between the points.

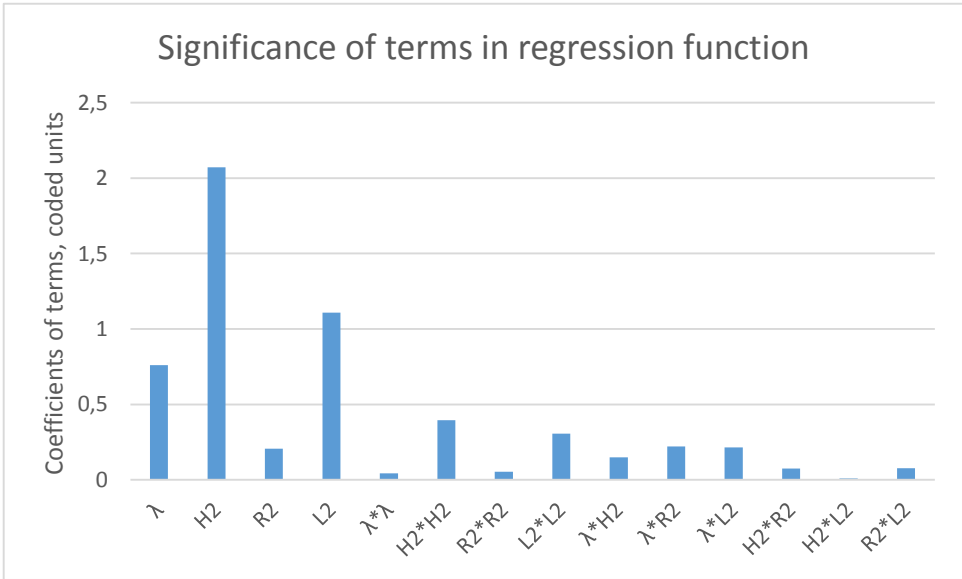


Figure 6.8 - Significance of terms, 1st Matrix, Hydrogen lance

Coded units					
Term	Coef	SE Coef	T	P	
Constant	38,1357	0,4263	89,466	0,000	
Lambda	-0,7597	0,2302	-3,300	0,005	
H2 fraction	2,0725	0,2302	9,003	0,000	
Ratio fuel S	0,2069	0,2302	0,899	0,382	
L2	1,1087	0,2302	4,816	0,000	
Lambda*Lambda	0,0430	0,2109	0,204	0,841	
H2 fraction*H2 fraction	-0,3952	0,2109	-1,874	0,079	
Ratio fuel S*Ratio fuel S	0,0527	0,2109	0,250	0,806	
L2*L2	0,3053	0,2109	1,448	0,167	
Lambda*H2 fraction	0,1501	0,2819	0,532	0,602	
Lambda*Ratio fuel S	0,2223	0,2819	0,789	0,442	
Lambda*L2	0,2153	0,2819	0,764	0,456	
H2 fraction*Ratio fuel S	0,0757	0,2819	0,269	0,792	
H2 fraction*L2	-0,0094	0,2819	-0,033	0,974	
Ratio fuel S*L2	-0,0765	0,2819	-0,271	0,790	

S = 1,12778	PRESS = 106,915
R-Sq = 88,57%	R-Sq(pred) = 39,94%
	R-Sq(adj) = 78,57%

Table 6.6 - Full quadratic model of 1st Matrix Hydrogen Lance

The full quadratic regression analysis of the data is presented in Table 6.6. All though the R²-value is good (88.57%), the R²-value predicted is only 39.94 percent, meaning that the model is very bad at predicting NO_x levels for other points than the observed. It indicates that the model is over-fitted. The lack-of-fit test gave a p-value less than 0.03. This means that the model does not fit the observations using a 95 % confidence level. To improve the regression function, all statistically insignificant terms were removed from the initial full quadratic model. The linear term of R2 (Ratio fuel S), as the p-value in Table 6.6 states, is not statistically significant and indicates that any trends from this factor can be of mere chance, but has to be included in the linear model.

$$NO_x = -12.156X_1 + 0.553X_2 + 0.138X_3 + 0.887X_4 + 27,908 \quad (17)$$

Coded units					
Term	Coef	SE Coef	T	P	
Constant	38,1402	0,1947	195,877	0,000	
Lambda	-0,7597	0,2213	-3,433	0,002	
H2 fraction	2,0725	0,2213	9,365	0,000	
Ratio fuel S	0,2069	0,2213	0,935	0,358	
L2	1,1087	0,2213	5,010	0,000	

S = 1,08413	PRESS = 46,4710
R-Sq = 82,83%	R-Sq(pred) = 73,90%
	R-Sq(adj) = 80,19%

Table 6.7 – Final model for 1st Matrix, Hydrogen lance

Only the linear terms were left in Table 6.7, which perhaps gives a less detailed picture of the characteristics of the burner. The model is not as robust as the other described in Table 6.3.

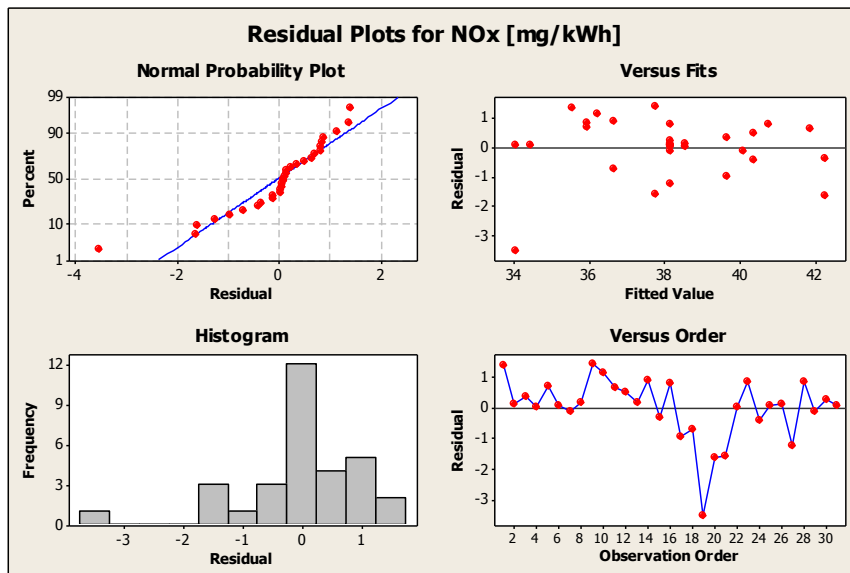


Figure 6.9 - Residual Plots, 1st Matrix, Hydrogen Lance

An outlier can be observed in the residual plots in Figure 6.9. It is observation number 19. Figure 6.7 states that observation number 19 was the only point with any significant increase in CO. The bottom right graph shows a variation of residuals over time. This experiment was conducted with wrong configuration, as discussed, and the flow rate of the cooler might have influenced the results.

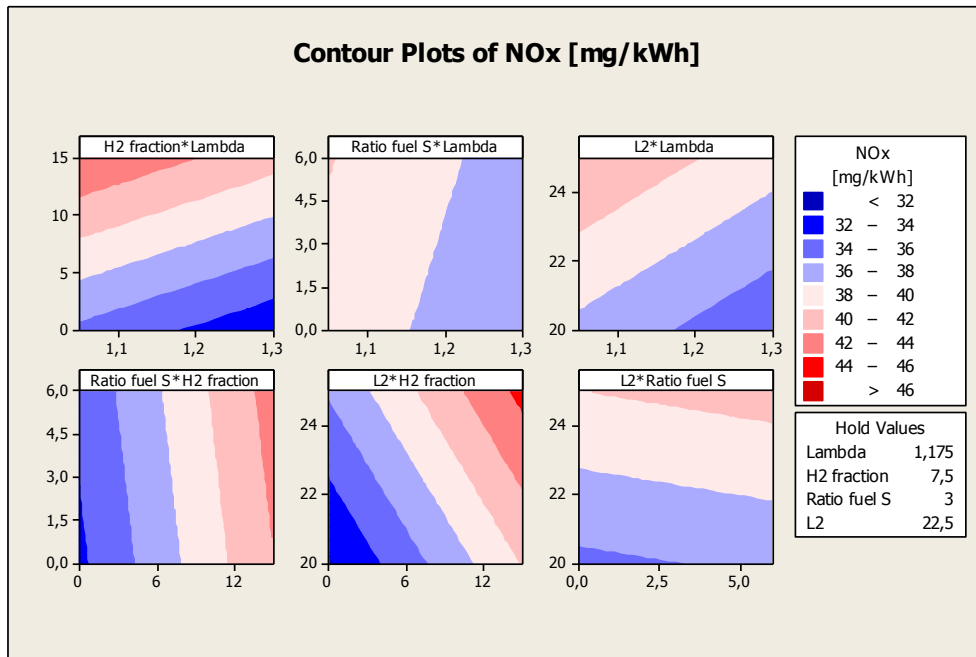


Figure 6.10 – Contour Plots for 1st Matrix, Hydrogen lance

The R^2 -value is lower, indicating the regression function does not fit the observed values in this experiment, as well as the previous. The predicted R^2 -value is now 73.90 %. This indicates that the model is better at predicting the NOx level than the analysis in Table 6.6. The lack-of-fit test for this model has a p-value of 0.059, which is greater than the α -limit of 0.05.

As mentioned, the trends due to different settings of R^2 should be ignored because of its statistical insignificance. Figure 6.10 shows the same trend of increasing NOx as more hydrogen is mixed into the fuel. By reducing the height of the burner head, L2, the NOx emissions tends to decrease, as was found in the previous experiment in Figure 6.5. Figure 6.10 shows that the emission levels decrease if more excess-air is provided to the flame.

6.2. The methane lance

The lance was already installed after preliminary test in 2012. The tests showed that the burned had to run at 20 kW or more for pure methane, in order to obtain full combustion with the current chamber. It was tested for the exactly same factors, ranges and power as the hydrogen lance.

6.2.1. 1st Matrix

As the burner operated at 25 kW during the whole experiment, acceptable amounts of CO were observed. Following results were obtained.

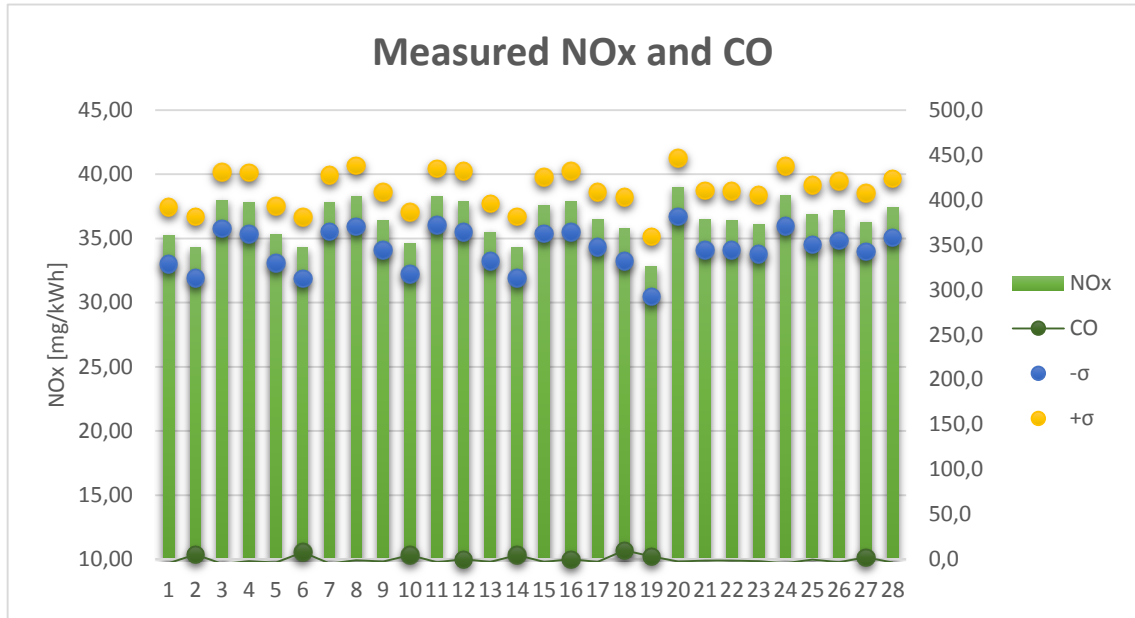


Figure 6.11 – Nox and CO, 1st Matrix Methane lance

The standard deviation of the measured NOx is great compared to the variation in the different measurement points. Only 28 of 31 points were measured for this experiment due to technical issues. The three remaining points were centre points and are implemented as stars (*) in Minitab. This allows the program to take into account that these values were not measured. They were all identical centre points. The intent is to repeat this point so that the model can get a grasp of the pure error in the experiment.

Coded Units					
Term	Coef	SE Coef	T	P	
Constant	36,9080	0,20355	181,325	0,000	
Lambda	-0,2553	0,08310	-3,073	0,009	
H2 fraction	1,4935	0,08310	17,973	0,000	
Ratio Fuel	-0,0654	0,08310	-0,787	0,445	
L2 Distance	0,2482	0,08310	2,987	0,010	
Lambda*Lambda	-0,1933	0,08310	-2,326	0,037	
H2 fraction*H2 fraction	-0,2442	0,08310	-2,938	0,012	
Ratio Fuel*Ratio Fuel	-0,1162	0,08310	-1,399	0,185	
L2 Distance*L2 Distance	0,0830	0,08310	0,999	0,336	
Lambda*H2 fraction	0,3186	0,10177	3,130	0,008	
Lambda*Ratio Fuel	0,1171	0,10177	1,150	0,271	
Lambda*L2 Distance	-0,0859	0,10177	-0,844	0,414	
H2 fraction*Ratio Fuel	0,0511	0,10177	0,502	0,624	
H2 fraction*L2 Distance	-0,1139	0,10177	-1,120	0,283	
Ratio Fuel*L2 Distance	-0,1391	0,10177	-1,367	0,195	

S = 0,407093 PRESS = 9,59995
R-Sq = 96,64% R-Sq(pred) = 85,02% R-Sq(adj) = 93,02

Table 6.8 – Full quadratic model for 1st Matrix, Methane lance

The results were first analysed for full quadratic model, presented in Table 6.8. The lack-of-fit of this model have a p-value of 0.75. In Table 6.8, many of the included terms are statistically insignificant. The terms with p-values larger than 0.05 were removed to improve the model. The regression function has to include four factors, so the linear term of R2 is included in the improved model even though its influence cannot be justified. The coefficient of the term, in coded unit, in the regression function is small compared to the other terms, as illustrated in Figure 6.12.

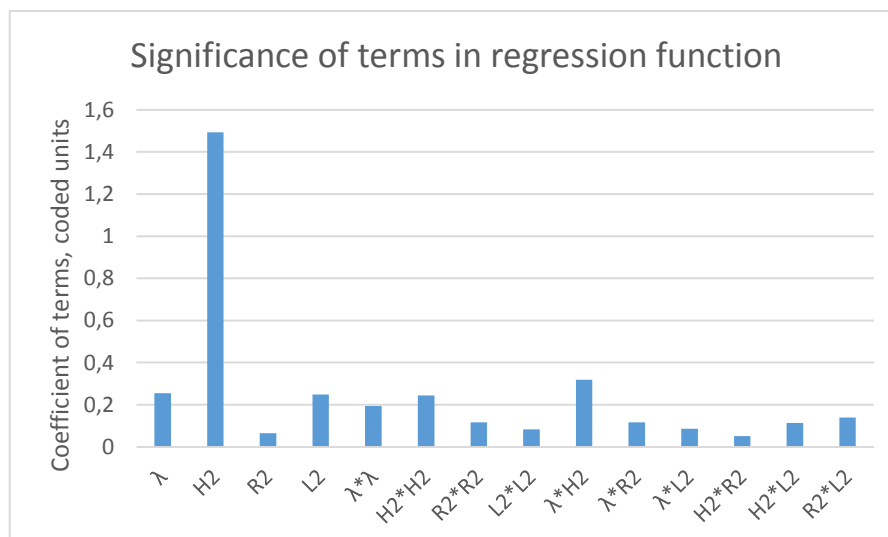


Figure 6.12 – Significance of terms, 1st Matrix, Methane lance

Coded Units					
Term	Coef	SE Coef	T	P	
Constant	36,8681	0,13595	271,182	0,000	
Lambda	-0,2553	0,08776	-2,910	0,009	
H2 fraction	1,4935	0,08776	17,019	0,000	
Ratio Fuel	-0,0654	0,08776	-0,745	0,465	
L2 Distance	0,2482	0,08776	2,828	0,010	
Lambda*Lambda	-0,1866	0,08325	-2,242	0,036	
H2 fraction*H2 fraction	-0,2375	0,08325	-2,853	0,010	
Lambda*H2 fraction	0,3186	0,10748	2,964	0,008	

S = 0,429922	PRESS = 6,65882
R-Sq = 94,23%	R-Sq(pred) = 89,61%
	R-Sq(adj) = 92,21%

Table 6.9 – Final model for 1st Matrix, Methane Lance

The improved model in Table 6.9 has a lower value of R^2 , but a higher value of the predicted R^2 . The p-value of the lack-of-fit test is 0.704. The improved model does not fit the observed values as well as the initial full quadratic model, but it is better at predicting new observations. The regression function in uncoded units is expressed in equation (18).

$$NO_x = -47,782X_1^2 - 0,017X_2^2 + 1,359X_1X_2 + 98,001X_1 - 0,946X_2 - 0,044X_3 + 0,199X_4 - 20,595 \quad (18)$$

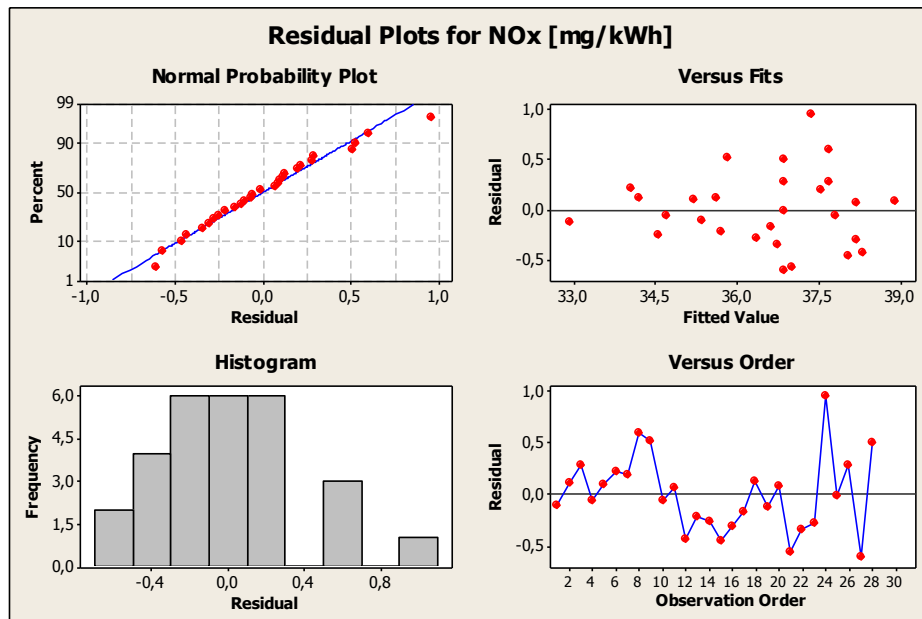


Figure 6.13 - Residual Plots, 1st Matrix, Methan Lance

Figure 6.13 shows that the residuals are normally distributed and with two outliers. The top right graph also illustrates an increasing variance for higher fitted values.

No certain information or trend from the factor R2 can be observed in Figure 6.14. As Figure 6.12 states, the domination of the factor H2 can be observed in contour plots. There is a reduction of emission for higher values of lambda, particularly for methane-rich fuels. No strong trend in emission of NOx can be observed for variation of lance positions L2 between 20 and 25 mm. In short, most of the variation of emission is observed in relation to variation of hydrogen content in the fuel.

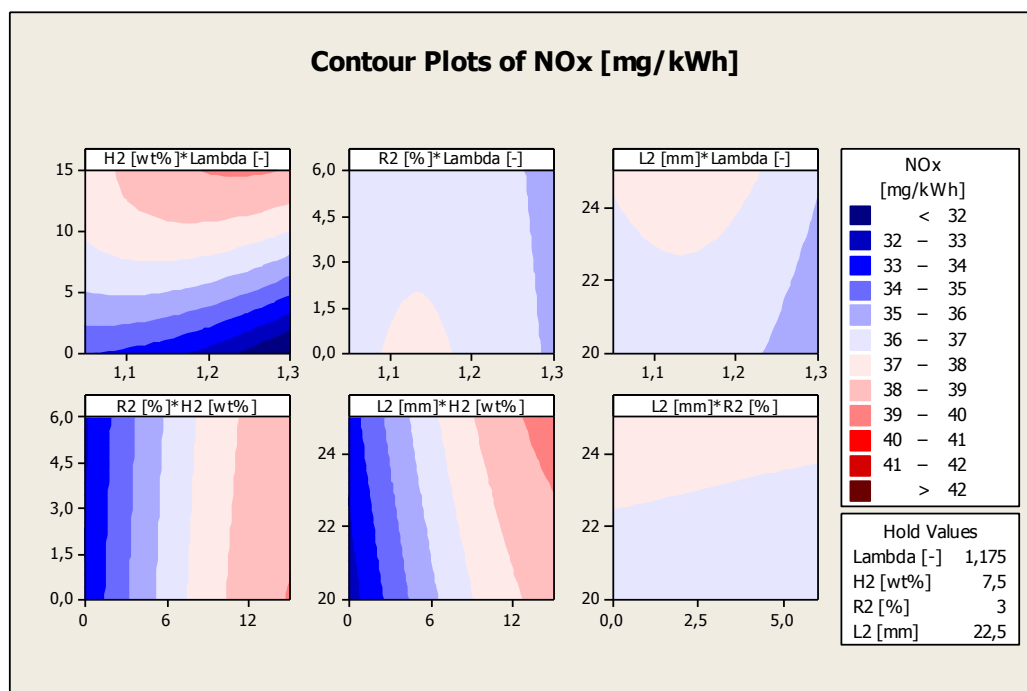


Figure 6.14 – Contour Plots for 1st Matrix, Methane lance

7. Discussion

All the statistical models presented in the result have their faults. The 2nd matrix provided maybe the clearest trends for the factors, but they have to be addressed carefully due to high concentrations of CO. The model presented for CO is qualitatively wrong in many ways, but do illustrate the area where higher CO emissions can be expected. As for the 1st matrix, the statistical robustness is questionable due to short ranges of the independent variables or factors. The response of NO_x emission did not vary enough compared to the expected pure error from measurement.

7.1. The 2nd matrix of the hydrogen lance

The reliability of the results from this experiment is good. The measurements were conducted with no leakages and all measurements were within the standard deviation of theoretical values. However, it was detected large amounts of CO for some measurement points. This most likely influenced the results. The large ranges of the factors gave clear differences in the response. These differences were considerably larger than the pure error the model measures from the centre points and may contribute to the high values of R^2 . Clear trends for each factor were observed.

7.1.1. R2 - Fuel to secondary holes

From the graphs in Figure 6.4, it is evident that any increase of fuel distributed to the secondary holes does not reduce the emission of NO_x, but rather increase the emission in many cases. The increase in R2 dampens the ability to reduce NO_x emission by lowering the L2 distance. The characteristics of the relationship between L2 and H2 change when most of the fuel is distributed to the primary holes. The emission of NO_x is lower overall, but reducing L2 seems to have a better effect in Figure 6.5. Tests run to map the upper ranges of secondary fuel suggests that the flame becomes less stable with increased values of R2, especially for pure methane. That is why the other experiments only test R2 up to five percent. This range was too narrow to give any effect on the emission of NO_x. The results from the first matrix, for both lances, could not tell anything about the influence from R2. The only information obtain about this factor is from the second matrix.

In short, fuel distribution to secondary holes does not seem to reduce the emission of NO_x, rather increase it and destabilise the flame.

7.1.2. L2 - Height of burner head

Significant differences in emission of NO_x were measured when adjusting the height of the burner head. Table 6.3 shows a strong linear effect between the NO_x emission and L2. The lower the distance of L2, the less emission of NO_x. This trend can be observed for all combinations of the three factors, although not as strong for the range tested in the first matrix (20-25 mm). The air outlet area is constant for values of L2 above 22 mm. The burner head is further up, but air will be provided at the same velocity. Figure 1.4 illustrates the maximum and minimum value for L2 to be 22 and 4.2 mm respectively. Between these values, the area varies from zero to maximum area of 368.2 mm².

This may explain why L2 does not influence the NO_x emission between 20 and 25 mm like in Figure 6.10; the air velocity did not change as much, only the position of the burner head.

For air at 260 l/min								
L2 [mm]	13	14	15	16	17	18	19	20
Velocity [m/s]	20,4	18,6	17,2	16,0	15,0	14,1	13,4	12,8

Table 6.10 - Velocity of air

Table 6.10 is based on equation (7) with the assumption that this experiment had an average airflow of 260 NI/min. It suggests that the air velocity was increased by approximately 60 % when adjusting the L2 distance from 20 mm to 13 mm. From section 1.2.3, it may be assumed that the NO_x emission is a function of the concentration of O-atoms and nitrogen, residence time and the peak temperature in the flame. The increased velocity may result in better mixing and reduce the peak temperature of the flame, thus reduce the emission of NO_x. At some point though, the flame temperature will be too low and full combustion is not sustained as Figure 6.6 indicates.

Another contribution may be shorter residence time. The amount of carbon monoxide measured for settings of low L2 and H2 in Figure 6.6 indicate that the residence time was too short for all the methane to burn with the given rate coefficient of the reaction. If the distance of L2 was increased, full combustion was eventually obtained. Full combustion may have been obtained due to increased residence time.

In preliminary tests, it was found that the flame became unstable at lower distances of L2 when burning pure methane. The flame was more stable when hydrogen was added, and the distance could be reduced further.

7.1.3. H2 – Mass fraction of hydrogen

Hydrogen addition to the fuel resulted in increased emission of NO_x, but it seems to stagnate as the amount reaches 30 percent of the weight (Figure 6.5). The results from the other experiments, where the first matrix was measured, show a trend of steady increase of NO_x as more hydrogen is added. These trends are hard to compare to the second matrix because the ranges of L2 do not overlap in the two studies. In the first matrix, the distance of L2 only ranged from 20 to 25 mm. The lance geometry is such that it influences the air inlet velocity for L2 between 4.2 mm and 22 mm. It is therefore possible that values of L2 greater than 22 mm is outside the scope of the variable. In any case, the overall trend is continuous increased NO_x emission when hydrogen is added for higher values of L2 (Figure 6.10) and converging values of NO_x for lower values of L2 (Figure 6.5). The results from the second matrix of the hydrogen lance have to be analysed with the notion that incomplete combustion may have influenced the results. There is a strong correlation between NO_x and CO emissions. The low values of NO_x in Figure 6.5, for low settings of hydrogen and L2, can be a result from incomplete combustion, thus a cooler flame temperature. Full combustion is obtained if more hydrogen is added to the fuel. This is likely due to hydrogen's high flammability that results in a much faster reaction. More energy and radicals are released within the residence time allowing full combustion of methane. The opposite effect is observed in other experiments for swirl burners (Cozzi and Coghe, 2006). Another way to avoid incomplete combustion is to increase the power. When the burner operates at higher power, like for the experiment based on the first matrix, no or little CO is observed. Future work should test the second matrix for higher power and compare the trend of NO_x emissions in the region where both L2 and H2 have low values.

A hydrogen mass fraction of maximum 30 percent was tested due to acoustic problems with the chamber. The acoustic noise was very bad for higher amounts of hydrogen, deforming the flame shape and causing an unbearable work-environment. Another combustion chamber with more appropriate dimensions should be designed in order to investigate high ranges of hydrogen content. Although it was found that it was possible to burn pure hydrogen without too much noise, the region in the middle makes it impossible to design any CCD for the whole range.

7.1.4. λ or Lambda – Amount of excess air

The second matrix did not include this factor, only the first matrix. The results from the hydrogen lance show a weak trend of reduction in NO_x as more air is provided. Stronger trends are illustrated in Figure 6.14 for the methane lance. The top left graph in the figure shows an interesting trend. The effect from increased lambda is stronger the more methane the fuel contains. There is barely any reduction in NO_x emission for fuel with 15 percent of hydrogen compared to pure methane when lambda goes from 1.05 to 1.3. The reduction is in any case no more than four milligrams per kilowatt-hour.

7.1.5. Power

Preliminary tests showed that the burner had to operate at 18 kW or more to obtain full combustion of pure methane. The first matrix was therefore chosen to operate at 25 kW. Using power as a variable was rejected due to practical reasons. The time to obtain steady-state temperature for each power prevented effective measurements. It was decided to run each experiment at constant power so that the temperature of the chamber also was kept constant. The measurements of the second matrix were conducted at 15 kW because of the small amounts of available fuel left. It was assumed that all the points would operate with full combustion, but that was not the case. As mentioned, it is therefore urged that the same combinations of factors are measured at a higher power.

7.2. The Two Lances

The same experiment was conducted for the two types of lances that came with the burner from Switzerland. The results of the experiments are presented in Figure 6.10 and Figure 6.14. Although the models are not very good, it can be argued that the same trends can be observed for the two experiments. The regression function for the hydrogen lance only contains linear terms while the function for the methane lance is quadratic. All settings were identical in both experiments, except the physical attribute of different fuel port diameters for the two lances. The results cannot point out any certain difference between the two lances. If the hard data for each point is compared, they follow the same trend, although with some deviations as would be expected. The fact that the different

points in the experiment produce almost the same amount of NO_x emission, it is harder to point out any clear trends. The pure error, or standard deviation, for each measurement is significant to the variations of emissions measured for different points in the experiment. It is advised that future experiments are conducted with factors with broader ranges, like the second matrix. Only then, when the pure error becomes negligible, the two lances can be compared.

It was noted another difference between the two lances. The hydrogen lance was able to sustain a flame for higher R₂ while burning pure methane. Where there was a flame blow out for the methane lance, the hydrogen lance could operate. This ability was however not looked into closer, as the goal was only to widen the range of the factors as much as possible.

7.3. Overall performance

It was not possible to investigate the burner for hydrogen content higher than 30 wt% due to problems with acoustic flame. In the tested range, the emission of NO_x lies between 30 and 50 milligram per kilo watt-hour. This corresponds to approximately 15 to 25 ppm in dry gas and is a good result compared to other burners in section 1.4. Figure 6.5 indicates that the increase in emission of NO_x stagnates for hydrogen content more than of 20% wt for same height of L₂. As the amount of hydrocarbon decrease in the fuel, less NO formation is expected, but to what degree is unknown. The thermal NO_x is most likely to be dominant. The same figure shows how strongly the height of L₂ affects the emission of NO_x. The low distance and increased flow velocity may suppress the thermal NO_x formation by reducing the residence time and peak temperature of the flame. The height of the burner was only tested down to 13 mm, but is capable of much lower height. The burner seem capable of counteract the increased temperature due to hydrogen-rich fuel by lowering L₂. Too low L₂ with methane-rich flame will cause incomplete combustion and eventually flame blow out. It is suspected this is due to the lower flammability of methane.

8. Conclusion

The partial premixed bluff-body burner had overall low emissions of NO_x (30-50 mg/kWh). This was not a quantitative study, but the values correspond to 15 to 25 ppm in exhaust with 3% O₂. It corresponds to other low-NO_x burners (Rørtveit et al., 2002). The height of the burner head (L2) is perhaps the dominant physical factor to influence the NO_x emission, besides fuel composition. Lower distances of L2 decrease the emission of NO_x, but also destabilise the flame for methane-rich fuels. This relationship should be investigated further in future studies. As the more hydrogen is present in the fuel, there is no certain trend. Some experiments indicate an increase in emission, while the 2nd matrix shows an increase first then a stagnation. The presence of CO in this experiment may have caused the trend, and it is suggested that the experiment should be repeated for higher power. This will exclude any CO emissions and the results can be compared. The experiments did not identify the dominant mechanism of NO_x formation. The distribution of fuel to the secondary fuel only contributed to instability and increased emissions. The intent of this design was not provided, so the factor may play a different role in other ranges of for example fuel composition. Some interesting trends for the burner are indicated with these central-composite designed experiments, but due to leakages and CO emissions, they are under doubt. Further experiment, without the issues described in this report, should be conducted to support the observed trends.

9. References

- ALICAT. *Alicat Mass Flow Controllers* [Online]. Available: <http://www.alicat.com/products/gas-flow/mass-flow-controllers/> [Accessed 21.05.2013].
- BERENDSEN, H. J. C. 2011. *A Student's Guide to Data and Error Analysis*. Cambridge: Cambridge University Press.
- BOX, G. E. P. & DRAPER, N. R. 1987. *Empirical model-building and response surfaces*, New York, Wiley.
- BOX, G. E. P., HUNTER, W. G. & HUNTER, J. S. 1978. *Statistics for experimenters: an introduction to design, data analysis, and model building*, New York, Wiley.
- BUHRE, B. J. P., ELLIOTT, L. K., SHENG, C. D., GUPTA, R. P. & WALL, T. F. 2005. Oxy-fuel combustion technology for coal-fired power generation. *Progress in Energy and Combustion Science*, 31, 283-307.
- COZZI, F. & COGHE, A. 2006. Behavior of hydrogen-enriched non-premixed swirled natural gas flames. *International Journal of Hydrogen Energy*, 31, 669-677.
- EPA. *EPA NOx - Health Issues* [Online]. Available: <http://www.epa.gov/airquality/nitrogenoxides/health.html> [Accessed 30.05.2013 2013].
- GASMET. *Gasmet FTIR* [Online]. Available: <http://www.gasmet.com/technologies/ftir> [Accessed 05.05.2013].
- MILLER, J. A. & BOWMAN, C. T. 1989. Mechanism and modeling of nitrogen chemistry in combustion. *Progress in Energy and Combustion Science*, 15, 287-338.
- MONTGOMERY, D. C., PECK, E. A. & VINING, G. G. 2012. *Introduction to linear regression analysis*, Hoboken, NJ, Wiley.
- MUZIO, L. J. & QUARTUCY, G. C. 1997. Implementing NOx control: Research to application. *Progress in Energy and Combustion Science*, 23, 233-266.
- MYERS, R. H., MONTGOMERY, D. C. & ANDERSON-COOK, C. M. 2011. *Response Surface Methodology : Process and Product Optimization Using Designed Experiments*. 3 ed. Chicester: Wiley.
- RØRTVEIT, G. J., ZEPTER, K., SKREIBERG, Ø., FOSSUM, M. & HUSTAD, J. E. 2002. A comparison of low-NOx burners for combustion of methane and hydrogen mixtures. *Proceedings of the Combustion Institute*, 29, 1123-1129.
- SKALSKA, K., MILLER, J. S. & LEDAKOWICZ, S. 2010. Trends in NOx abatement: A review. *Science of The Total Environment*, 408, 3976-3989.
- SPANGELO, Ø. 2004. *Experimental and theoretical studies of a low NOx swirl burner*. Norwegian University of Science and Technology.
- WARNATZ, J., MAAS, U. & DIBBLE, R. W. 2006. *Combustion: Physical and Chemical Fundamentals, Modeling and Simulation, Experiments, Pollutant Formation*, Berlin, Heidelberg, Springer Berlin Heidelberg.
- YEGIAN, D. T. & CHENG, R. K. 1998. Development of a Lean Premixed Low-Swirl Burner for Low NOx Practical Applications. *Combustion Science and Technology*, 139, 207-227.

10. Appendix

All appendices are provided digitally in following order.

A – DATA

All data from measurements in their raw form.

B – Calculations

All calculations of the data from the experiments.

C – Minitab Projects

All projects that were used in analysis of the results from calculations of the data.

D – Movie of flame shape

A movie illustrating the effect of the factor L2. Please loop movie in media player.

E – PPBB drawings

Technical drawings of the burner.

F – MFC calibration 2013

Excel sheets with the result from calibration of the mass flow controllers 2013.